Taking $\Delta_{pp'} \gg \hbar\omega_c$, $\hbar^2(\omega_k \pm \omega_{k'})$ may be neglected in the denominators of (B4). Using this result in (B3) gives, on dropping the terms involving $\sin(k \pm k')R$,

$$\mathcal{H}_o''^{(2)} = \frac{9\alpha_{10}^2(4\hbar)^3|\langle p|rY_{10}|p'\rangle|^2}{(a^4MN\Delta_{pp'})^2} \sum_{j,j'=1}^{\infty} \frac{(-1)^{j+j'}}{(jj')^4} \sum_{k,k'} \left[\frac{(n_{k'}+\frac{1}{2})}{\omega_{k'}} + \frac{(n_k+\frac{1}{2})}{\omega_k}\right]$$

$$\times \cos(kR)\cos(k'R)\sin(kja)\sin^2(\tfrac{1}{2}k'ja)\sin(kj'a)\sin^2(\tfrac{1}{2}k'j'a). \quad \text{(B5)}$$

$\mathcal{H}_e''^{(2)}$ is obtained in a similar way and is given in Eq. (21) in the main text.

PHYSICAL REVIEW B VOLUME 1, NUMBER 4 15 FEBRUARY 1970

Phonon Optical Properties of $Ca_{1-x}Sr_xF_2$†‡

W. B. LACINA* AND P. S. PERSHAN
Division of Engineering and Applied Physics, Harvard University, Cambridge, Massachusetts 02138
(Received 22 August 1969)

The phonon optical properties of the mixed fluorite system $Ca_{1-x}Sr_xF_2$ are treated theoretically using the "average-Green's-function" formalism. The calculations are based on a rigid-ion model for the pure CaF_2 lattice, with a defect model for Sr^{++} impurities that includes both mass and force-constant changes. Results are compared with experimental observations on Raman scattering and far-infrared reflectivity spectra.

I. INTRODUCTION

THE general problem of the effects of impurities on the vibrational, electronic, and magnetic properties of crystalline solids has currently attracted much interest. One aspect of this problem has been the study of random disordered systems, and in recent years, there have been numerous experimental and theoretical investigations of the phonon optical properties of mixed crystal systems. We have studied experimentally[1] the Raman scattering (at ~4, 77, and 300°K) from the mixed fluorite systems $Ca_{1-x}Sr_xF_2$ and $Ba_{1-x}Sr_xF_2$ using laser excitation and a photon-counting detection system. Analogous work on the far-infrared reflectivity spectra for these systems has been carried out by Verleur and Barker.[2] In this paper we shall present a detailed discussion of the numerical methods used, and the results obtained, in an analysis of this experiment. A partial account of some of these results has appeared previously.[3]

The Green's-function methods which have been extensively employed for the isolated defect and random disorder problems are briefly reviewed in Sec. III, where it will be shown how the phonon optical properties can be expressed using this formalism. These techniques have been very useful for qualitative and quantitative understanding of impurity effects, although they usually involve cumbersome computational difficulties for physically realistic models of the impurity and the host lattice. A low concentration theory for Raman scattering and infrared absorption in mixed crystals, based on an average Green's function $\langle \mathbf{G} \rangle$, is described and applied to the $Ca_{1-x}Sr_xF_2$ system in Sec. IV; theoretical calculations are presented and compared with experimental measurements. The "proper self-energy" (PSE) functions which arise in this formalism are calculated to first order in the concentration x, and involve certain unperturbed phonon Green's functions $G_{\alpha\beta}{}^0(l\kappa, l'\kappa'; \omega+i\epsilon)$ which have been computed numerically for CaF_2, using a rigid-ion model of a harmonic fluorite lattice. Some of these Green's functions, as well as some of the details concerning their computation, have been included in the Appendix, since it is likely that they would be useful for many other studies of phonon impurity problems involving CaF_2. For example they could also be applied to problems of defect-induced Raman scattering or infrared absorption from U centers, to vibrational sidebands in electronic fluorescence spectra, to neutron scattering, etc.

The literature in this field has been expanding so rapidly that it would be futile to attempt to cite all of the work that has been done. An excellent and extremely

† Work supported in part by the Advanced Research Projects Agency, by the Joint Services Electronics Program (U. S. Army, U. S. Navy, and U. S. Air Force) under Contract No. Nr-1866(16), and by the Division of Engineering and Applied Physics, Harvard University.

‡ Based on part of the Ph.D. thesis of W. B. Lacina, Harvard University, 1969 [Technical Report No. ARPA-36 (unpublished)].

* Present address: Northrop Corporate Laboratories, Hawthorne, Calif. 90250.

[1] R. K. Chang, B. Lacina, and P. S. Pershan, Phys. Rev. Letters **17**, 755 (1966).

[2] H. W. Verleur and A. S. Barker, Jr., Phys. Rev. **164**, 1169 (1967); Solid State Commun. **5**, 695 (1967).

[3] P. S. Pershan and W. B. Lacina, in *Light Scattering Spectra of Solids*, edited by G. B. Wright (Springer-Verlag, New York, 1969), p. 439.

thorough review article on the effects of point defects and disorder on lattice vibrational properties has been given by Maradudin.[4] The experimental literature on phonon optical properties in mixed crystal systems is extensive; several examples of other systems that have been studied by Raman scattering and infrared absorption include $GaAs_{1-x}Sb_x$,[5] $Ni_{1-x}Co_xO$,[6] $Zn_{1-x}Cd_xS$,[7] $ZnSe_{1-x}Te_x$,[8] $Na_{1-x}K_xCl$,[9] $K_{1-x}Rb_xCl$,[10] $KCl_{1-x}Br_x$,[10,11] $K_{1-x}Rb_xI$,[11] $KMg_{1-x}Ni_xF_3$,[12] $Na_{1-x}K_xTaO_3$,[13] $KTa_{1-x}Nb_xO_3$,[13] $Si_{1-x}Ge_x$,[14] $InP_{1-x}As_x$,[15] $GaP_{1-x}As_x$,[16-18] $CdS_{1-x}Se_x$,[19-22] $ZnS_{1-x}Se_x$,[23] $NaCl_{1-x}{}^{35}Cl_x{}^{37}$,[24] and $LiH_{1-x}D_x$.[25] There would be many more examples if the list were enlarged to include work on other than phonon optical properties. There are also some general articles which are a useful review of the experimental results on mixed crystal systems[26] and a discussion of the behavior of the long wavelength optical modes.[27]

Experimental observations on Raman scattering and infrared absorption from such crystals has yielded, basically, two characteristic types of behavior. Assume that a mixed crystal $A_{1-x}B_xC$ can be formed as an alloy of pure AC and pure BC, each of which is characterized by one optically active mode with frequencies ω_A and ω_B, respectively. Then, in the first (type-I) behavior, the mixed crystal $A_{1-x}B_xC$ continues to exhibit[1,2,5-13] a *single* $\mathbf{k}\sim 0$ optic mode which shifts linearly with the concentration x from the frequency ω_A (that characterizes pure AC) to ω_B (that for pure BC). The intensity of the mode remains approximately constant, and the linewidth increases and peaks near the center ($x\sim 0.5$) of the mixture. For the second (type-II) behavior,[14-24] the mixed crystal exhibits two modes which are close to those which characterize pure AC and pure BC. The intensity of these modes varies in approximate proportion to the fraction of each component present. As the (molar) concentration x increases, the intensity of the BC mode increases, while that of AC decreases, with both shifting slightly.

It is possible for some modes of a crystal to exhibit behavior intermediate between types I and II, and it is also possible for different modes of the *same* mixed crystal system to display different behaviors. The formulation of a theory of the optical phonon properties of a mixed crystal system in terms of average Green's functions can provide[28] a criterion for the "virtual-crystal approximation" that characterizes the linear shift (type-I) behavior, and is also capable of explaining the "local-mode" behavior that characterizes type-II spectra.

II. EXPERIMENTAL DATA

We have measured experimentally the linewidths and frequency shifts for the first-order Raman active phonon mode in the mixed fluorite systems $Ca_{1-x}Sr_xF_2$ and $Ba_{1-x}Sr_xF_2$ for a variety of concentrations from $x=0$ to $x=1$. These crystals, which have long been known to form continuous solid solutions,[29,30] were obtained from Optovac, Inc. The crystal samples were excited by a cw gas laser source, and the method of detection employed a photon-counting technique. Light scattered at right angles from the laser beam was focused onto the entrance slit of a grating monochrometer, which was equipped with a motor drive for scanning the spectrum wavelength at a constant rate. Signal pulses from a phototube, placed at the exit slit of the monochrometer, were fed into a Nuclear Chicago RIDL Model No. 34-12B multichannel analyzer. This instrument was used in the "time base" mode of operation—all of the pulses that arrive from the phototube, in a preselected interval of time, are counted and stored sequentially in 400 channels. Thus, as the wavelength is scanned

[4] A. A. Maradudin, in *Solid State Physics*, edited by F. Seitz and D. Turnbull (Academic Press Inc., New York, 1966), Vol. 18, p. 278; Vol. 19, p. 1.

[5] R. F. Potter and D. L. Stierwalt, in *Proceedings of the International Conference on the Physics of Semiconductors, Paris, 1964* (Academic Press Inc., New York, 1965), p. 1111.

[6] P. J. Gielisse, J. N. Plendl, L. C. Mansur, R. Marshall, S. Mitra, R. Mykolajewycz, and A. Smakula, J. Appl. Phys. **36**, 2446 (1965).

[7] G. Lucovsky, E. Lind, and E. A. Davis, in *Proceedings of the International Conference on the Physics of II-VI Semiconductors* (W. A. Benjamin, Inc., New York, 1967); O. Brafman and S. S. Mitra, Phys. Rev. **171**, 931 (1968).

[8] O. Brafman, I. F. Chang, and S. S. Mitra (unpublished); cf. Ref. 23 below.

[9] F. Kruger, O. Reinkober, and E. Koch-Holm, Ann. Physik **85**, 110 (1928).

[10] A. Mitsuishi (unpublished); cf. Ref. 23.

[11] J. H. Fertel and C. H. Perry, Phys. Rev. (to be published).

[12] A. S. Barker, J. A. Ditzenberger, and H. J. Guggenheim, Phys. Rev. **175**, 1180 (1968).

[13] C. H. Perry and N. E. Tornberg, in *Light Scattering Spectra of Solids*, edited by G. B. Wright (Springer-Verlag, New York, 1969), p. 467.

[14] D. W. Feldman, M. Ashkin, and J. H. Parker, Phys. Rev. Letters **17**, 1209 (1966).

[15] F. Oswald, Z. Naturforsch. **14a**, 374 (1959).

[16] Y. S. Chen, W. Shockley, and G. L. Pearson, Phys. Rev. **151**, 648 (1966).

[17] H. W. Verleur and A. S. Barker, Jr., Phys. Rev. **149**, 715 (1966).

[18] N. D. Strahm and A. L. McWhorter, in *Light Scattering Spectra of Solids*, edited by G. B. Wright (Springer-Verlag, New York, 1969), p. 455.

[19] M. Balkanski, R. Beserman, and J. M. Besson, Solid State Commun. **4**, 201 (1966).

[20] J. Parrish, C. H. Perry, O. Brafman, I. F. Chang, and S. S. Mitra, in *Proceedings of the International Conference on the Physics of II-VI Semiconductors* (W. A. Benjamin, Inc., New York, 1967).

[21] H. W. Verleau and A. S. Barker, Jr., Phys. Rev. **155**, 750 (1967).

[22] J. M. Ralston, D. E. Keating, and R. K. Chang, in *Light Scattering Spectra of Solids*, edited by G. B. Wright (Springer-Verlag, New York, 1969), p. 369.

[23] O. Brafman, I. F. Chang, G. Lengyel, S. S. Mitra, and E. Carnall, Phys. Rev. Letters **19**, 1120 (1967); in *Proceedings of the International Conference on Localized Excitations in Solids* (Plenum Press, Inc., New York, 1968).

[24] M. V. Klein and H. F. MacDonald, Phys. Rev. Letters **20**, 1031 (1968).

[25] S. S. Jaswal and J. R. Hardy, Phys. Rev. **171**, 1090 (1968).

[26] G. Lucovsky, E. Burstein, and M. Brodsky, in *Proceedings of the International Conference on Localized Excitations in Solids* (Plenum Press, Inc., New York, 1968).

[27] I. F. Chang and S. S. Mitra, Phys. Rev. **172**, 924 (1968).

[28] P. S. Pershan and W. B. Lacina, Phys. Rev. **168**, 725 (1968).

[29] E. Rumpf, Z. Physik. Chem. (Leipzig) **B7**, 148 (1930).

[30] E. G. Chernevskaya and G. V. Anan'eva, Fiz. Tverd. Tela **8**, 216 (1966) [English Transl.: Soviet Phys.—Solid State **8**, 169 (1966)].

linearly by the motor-driven grating, the RIDL channel address advances linearly in discrete time intervals; the result is that the spectrum is stored digitally in the 400 channels of the analyzer. The RIDL channel width is variable with discrete values, and typically, a width of 1 or 2 sec was used. Furthermore, in order to improve signal-to-noise characteristics, it is often desirable to scan the same spectral range over and over, and add up the results. One of the advantages of the present method of detection is that this can be easily done, since the RIDL is capable of adding a new spectrum to one already stored in its memory. Thus, by means of an electromechanical control device that was specially designed to provide this multiple-scan feature, it was possible to obtain very clean data by improved signal-to-noise.

The earliest measurements[1] were made using a 1-m Jarrell Ash Model 78-420 spectrometer, a Spectra Physics Model 116 helium neon laser (6238 Å, ~25 mW) an Amperex XP1002 phototube (S-20), and a lab-built cold-finger helium Dewar. Later measurements were taken on a similar setup which included a Spex Model 1400 double monochrometer, a lab-built ionized argon laser (4880 Å, ~200 mW), an EMI 9558 phototube (S-20), and a Janis Super Vari-Temp Model 10-DT helium gas-cool Dewar. Because the fluorite systems studied here exhibit first-order Raman frequency shifts on the order of ~300 cm^{-1}, the separation from the laser line is far enough that the problem of extraneous light scattering in the Jarrell Ash spectrometer could be eliminated by using a dielectric interference filter at the entrance slit to reject the laser light. For the Spex double monochrometer, the scattering problem is significantly reduced, and such a filter for eliminating the laser line was not necessary when that system was used.

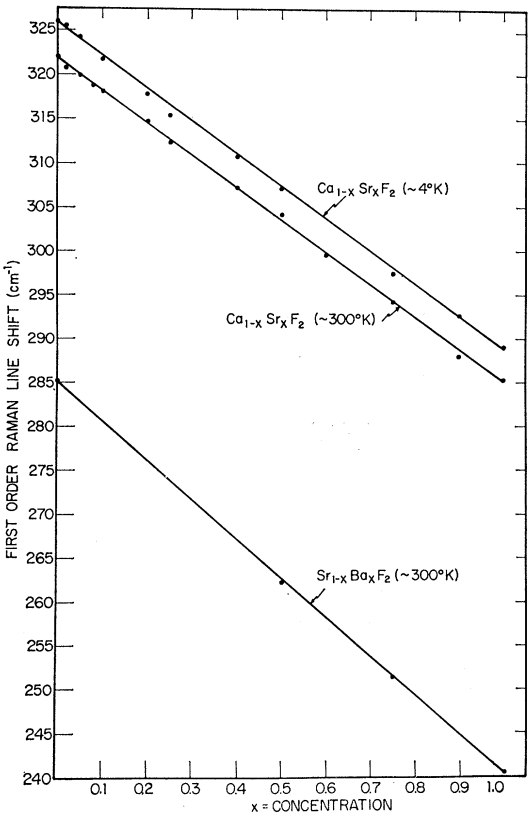

FIG. 1. First-order Raman line shifts for $Ca_{1-x}Sr_xF_2$ and $Sr_{1-x}Ba_xF_2$.

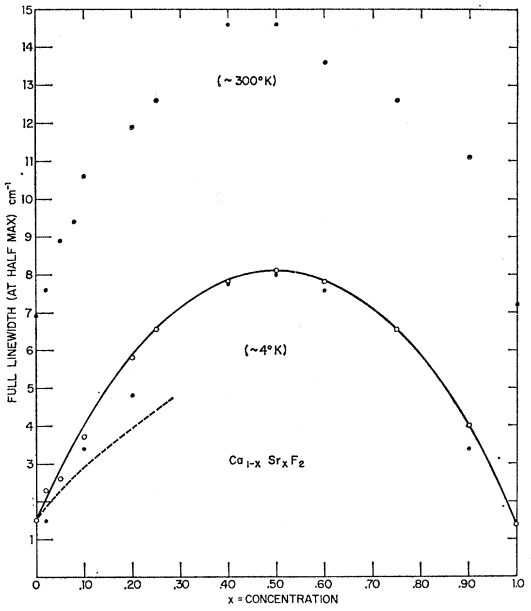

FIG. 2. Full linewidths (at half-maximum) for the $Ca_{1-x}Sr_xF_2$ system. Experimental points are the actual widths after convolution; dashed lines is theoretical. Open circles correspond to the 4880 Å data, and closed to the 6328 Å data.

The experimental results for the $Ca_{1-x}Sr_xF_2$ and $Sr_{1-x}Ba_xF_2$ mixed crystal systems are shown in Figs. 1 and 2; the first-order $\mathbf{k}\sim 0$ Raman line shifts linearly with the concentration, with an integrated intensity that remains approximately constant, and with a linewidth that increases and peaks at the 50-50 mixture. Because Raman scattering intensities are typically very low, it was necessary to use relatively large spectrometer slit openings for studying these systems. (For the Jarrell Ash spectrometer and 6328 Å laser, ~3.9-cm^{-1} slit; and for the Spex double monochrometer and 4880 Å laser, ~1.6-cm^{-1} slit.) In order to obtain *actual* linewidth results, it is then necessary to convolute the observed line profiles with the "slit function," which can be inferred experimentally from an observation of the laser line spectrum with the same slits. Theoretically (for curved slits, or for straight slits with small vertical aperture) the slit function should be a triangle. However, in practice, the slit function for the Jarrell Ash (which has curves slits) had a small flat top, and that for the Spex (with straight slits) had a small tail on one side, but was otherwise approximately triangular. In order to deconvolute the experimental results, it was

assumed that, in both cases, the slit function could be represented as approximately trapezoidal. It is important to note that it is not possible merely to subtract the instrumental width from observed linewidths when the slits are opened wide.

The low-temperature (~4°K) linewidth data were taken using both the 4880 and 6328 Å setups, and after the appropriate convolution corrections, the results of the two sets of measurements were reasonably consistent (cf. Fig. 2). Taking into account the experimental error in reading the data, as well as the error associated with the convolution process, these values are probably accurate to about $\sim\pm 0.3$ cm^{-1}, with a systematic discrepancy of ~ 0.3 cm^{-1} in the two sets of measurements. Taking into consideration that the two sets of data were taken at different times (approximately one year apart) and with completely different equipment, a systematic error of that magnitude does not seem too large. The source of that error is most likely in the assumptions made for the shape of the slit function, which could easily lead to an error of that magnitude when the two sets of data are reduced by convolutions with different slit functions. (It is *not* likely that this discrepancy is a real effect, related to excitation with 4880 or 6328 Å.) The linewidth *shift* $\delta\Gamma=\Gamma_R(x)-\Gamma_R(0)$ for the two sets of measurements is consistent, with an error of ~ 0.3 cm^{-1}, and it is this quantity that shall be important for the later comparison of theory with experiment. The theory of the $Ca_{1-x}Sr_xF_2$ mixed crystal system to be discussed in Sec. IV is only able to predict the *additional* contribution that disordering makes to the linewidth; thus, it is only the *change* in linewidth with concentration that concerns us here. The dashed line of Fig. 2 is the result of a numerical calculation (to be described below) in which the linewidth at zero concentration is arbitrarily set equal to the measured one.

Some data were also taken at liquid-nitrogen temperature, and within the experimental error, the results for the shifts and linewidths were about the same at ~4 and ~77°K.

III. BASIC THEORY

Quantum-mechanical double-time Green's-function methods have provided a useful approach to the study of properties of crystalline solids containing impurities.[4,31–48] These mathematical techniques can be successfully applied to the "isolated impurity" problem whenever the perturbation caused by the defect is spatially localized. Because of their generality, Green's-function techniques can be used to describe a wide variety of impurity effects on the physical properties of solids; the underlying unity that characterizes these methods allows the mathematical formulation of many physically diverse phenomena to be carried out in essentially the same way.[31] For the lattice vibrational problem, there are several excellent review articles available by Maradudin,[4,32,33] Elliott *et al.*,[34–36] Kwok,[37] and others. We shall discuss only some of the basic aspects of the Green's-function formalism here, since much of this theory is thoroughly treated in the literature. The main purpose of a short review here is to establish notation and to provide a background for the calculations that are described in Sec. IV below.

Because the problem of a single impurity is now reasonably well understood, much of the current interest in the properties of defects has shifted to studies of mixed crystal systems. The most extensive theoretical work on random disordered crystals has consisted of attempts to extend those methods of Green's functions which have proved so successful for describing the isolated local impurity problem. These "average-Green's-function" techniques[28,44–48] have been fruitful for explaining many of the features of a disordered system, although they are often limited by the approximations that must be imposed for even the simplest models. In some respects, these approximations have not been completely satisfactory; for example, they are inadequate for explaining many of the complicated "spike" effects which exact machine solutions have shown[49–55] can exist for even the simplest systems. Part of the difficulty

[31] Y. A. Izyumov, Advan. Phys. **14**, 569 (1965).
[32] A. A. Maradudin, in *Astrophysics and the Many-Body Problem* (W. A. Benjamin, Inc., New York, 1963); in *Phonons and Phonon Interactions*, edited by T. A. Bak (W. A. Benjamin, Inc., New York, 1964).
[33] A. A. Maradudin, Rept. Progr. Phys. **28**, 331 (1965).
[34] R. J. Elliott and D. W. Taylor, Proc. Roy. Soc. (London) **A296**, 161 (1967).
[35] R. J. Elliott, in *Phonons in Perfect Lattices and in Lattices with Point Imperfections*, edited by R. W. H. Stevenson (Plenum Press, Inc., New York, 1966); in *Proceedings of the International Conference on Lattice Dynamics, Copenhagen, Denmark, 1963*, edited by R. F. Wallis (Pergamon Press, Ltd., Oxford, 1965).
[36] R. J. Elliott, Argonne Natl. Laboratory Report No. ANL-7237, 1966 (unpublished).
[37] P. C. K. Kwok, in *Solid State Physics*, edited by F. Seitz and D. Turnbull (Academic Press Inc., New York, 1968), Vol. 20, p. 213.
[38] D. N. Zubarev, Usp. Fiz. Nauk **71**, 71 (1960) [English Transl.: Soviet Phys.—Usp. **3**, 320 (1960)].
[39] I. M. Lifshitz, Advan. Phys. **13**, 483 (1964).
[40] G. Benedek and G. F. Nardelli, Phys. Rev. **155**, 1004 (1967).
[41] M. V. Klein, Phys. Rev. **131**, 1500 (1963); **141**, 716 (1966).
[42] F. Yonezawa and T. Matsubara, Progr. Theoret. Phys. (Kyoto) **35**, 357 (1966).
[43] T. Wolfram and J. Callaway, Phys. Rev. **130**, 2207 (1963).
[44] J. S. Langer, J. Math. Phys. **2**, 584 (1961).
[45] H. Poon and A. Bienenstock, Phys. Rev. **141**, 7105 (1966); **142**, 466 (1966).
[46] P. L. Leath and B. Goodman, Phys. Rev. **148**, 968 (1966); **175**, 963 (1968).
[47] R. W. Davies and J. S. Langer, Phys. Rev. **131**, 163 (1963).
[48] D. W. Taylor, Phys. Rev. **156**, 1017 (1967).
[49] P. Dean, Proc. Phys. Soc. (London) **73**, 413 (1959); Proc. Roy. Soc. (London) **A254**, 507 (1960); **A260**, 263 (1961).
[50] P. Dean and J. L. Martin, Proc. Roy. Soc. (London) **A259**, 409 (1960).
[51] P. Dean and M. D. Bacon, Proc. Phys. Soc. (London) **81**, 642 (1963).
[52] J. L. Martin, Proc. Roy. Soc. (London) **A260**, 139 (1961).
[53] M. D. Bacon, P. Dean, and J. L. Martin, Proc. Phys. Soc. (London) **80**, 174 (1962).
[54] H. B. Rosenstock and R. E. McGill, J. Math. Phys. **3**, 200 (1962).
[55] D. N. Payton, III, and W. M. Visscher, Phys. Rev. **154**, 802 (1967); **156**, 1032 (1967); **175**, 1201 (1968).

arises because the approximations that are introduced make tacit assumptions about the analytic behavior of the average Green's function as a function of the concentration x. Except for some "self-consistent" analyses,[42,47,48] the usual approach is to expand the inverse of the average Green's function $\langle \mathbf{G}(x)\rangle^{-1}$ as a power series in x (which requires assumptions about analyticity properties). Even in situations where such approximations can be applied with reasonable assurance of validity, tedious numerical calculations are usually involved for realsitic models of the lattice and defect which make it difficult to evaluate $\langle \mathbf{G}(x)\rangle^{-1}$ beyond first order in x. Nevertheless, despite some of these shortcomings, these techniques have had great success in describing many of the impurity effects observed in physical systems.

In this section, a summary of the Green's-function methods that are applicable to the lattice dynamics of a random, disordered crystal will be given. The rigid-ion model in the harmonic approximation will be described, and it will be shown how Raman scattering and infrared absorption are related to certain phonon Green's functions. The results of numerical calculations for the $Ca_{1-x}Sr_xF_2$ system will be given in Sec. IV.

A. Lattice Dynamics

In the harmonic approximation (to which the present work shall be restricted) the vibrational Hamiltonian of a crystal lattice can be written[56,57]

$$\mathcal{H}=\tfrac{1}{2}\sum_{l\kappa\alpha} M_{l\kappa}\dot{u}_\alpha(l\kappa)^2+\tfrac{1}{2}\sum_{l\kappa\alpha,l'\kappa'\beta} u_\alpha(l\kappa) \times\Phi_{\alpha\beta}(l\kappa,l'\kappa')u_\beta(l'\kappa'), \quad (1)$$

where $u_\alpha(l\kappa)$ represents the α component of the displacement from equilibrium of the atom with cell index l and basis index κ. For a *perfect* lattice, the force constants $\Phi_{\alpha\beta}{}^0(l\kappa,l'\kappa')$ depend only upon $(\mathbf{R}_{l'\kappa'}-\mathbf{R}_{l\kappa})$, and the masses $M_{l\kappa}{}^0$ are independent of the cell index l. In an obvious matrix notation, the Hamiltonian for a perfect lattice is given by

$$\mathcal{H}_0=\tfrac{1}{2}\dot{\mathbf{Q}}^T\dot{\mathbf{Q}}+\tfrac{1}{2}\mathbf{Q}^T\mathbf{D}^0\mathbf{Q}, \quad (2)$$

where $\mathbf{D}^0=\mathbf{M}_0{}^{-1/2}\mathbf{\Phi}^0\mathbf{M}_0{}^{-1/2}$ is called the *dynamical matrix*, and the (column) matrix $\mathbf{Q}$ is defined by $\mathbf{Q}=\mathbf{M}_0{}^{1/2}\mathbf{u}$. The eigenvectors of the Hermitian matrix $\mathbf{D}^0$ are the phonon normal modes, $|\mathbf{k}\sigma\rangle$, where $(\mathbf{k},\sigma)$ labels the momentum and branch index:

$$\mathbf{D}^0|\mathbf{k}\sigma\rangle=\omega_{\mathbf{k}\sigma}{}^2|\mathbf{k}\sigma\rangle. \quad (3)$$

The relation between the basis vectors $|l\kappa\alpha\rangle$ of the "crystal lattice site" representation and the vectors $|\mathbf{k}\sigma\rangle$ of the "momentum space" representation can be expressed concisely by the transformation function

$$\langle l\kappa\alpha|\mathbf{k}\sigma\rangle=N^{-1/2}e^{i\mathbf{k}\cdot\mathbf{R}_{l\kappa}}w_\alpha(\kappa|\mathbf{k}\sigma), \quad (4)$$

where the set of vectors $w_\alpha(\kappa|\mathbf{k}\sigma)$ are eigenvectors of the Fourier-transformed dynamical matrix

$$D_{\alpha\beta}{}^0(\mathbf{k}|\kappa\kappa')=\sum_l e^{-i\mathbf{k}\cdot(\mathbf{R}_{l\kappa}-\mathbf{R}_{l'\kappa'})}D_{\alpha\beta}{}^0(l\kappa,l'\kappa'), \quad (5)$$

$$\sum_{\kappa'\beta} D_{\alpha\beta}{}^0(\mathbf{k}|\kappa\kappa')w_\beta(\kappa'|\mathbf{k}\sigma)=\omega_{\mathbf{k}\sigma}{}^2w_\alpha(\kappa|\mathbf{k}\sigma). \quad (6)$$

In order to evaluate the phonon eigenfrequencies $\omega_{\mathbf{k}\sigma}$ and eigenvectors $w_\alpha(\kappa|\mathbf{k}\sigma)$ (which shall be needed in later calculations of phonon Green's functions), it is necessary to construct a model of the lattice. These quantities shall be evaluated for CaF_2 by using a rigid-ion model, due to Ganesan and Srinivasan,[58] for the (ionic) fluorite lattice. The crystal is regarded as consisting of a lattice of rigid, nonpolarizable ions which interact through long-range electrostatic and short-range repulsive forces. The short-range interaction terms, whose physical origin is a repulsion between overlapping electronic distributions, fall off rapidly with distance, and are included only for nearest neighbors in the present model. The Coulomb forces between ions are assumed to be electrostatic interactions between rigidly spherical charge distributions (i.e., "point charges") that are multiples of an effective electronic charge Ze. A more complete description of the physics of the rigid-ion model, and of the successes it has for predicting various experimental quantities, can be found in the original source.[58] The formal details that are relevant to the present calculations of phonon eigenfrequencies and eigenvectors shall be described in more detail here.

For fluorite structure, shown in Fig. 3, the space group is $O_h{}^5$-*Fm3m*. The crystal consists of three interpenetrating *fcc* lattices, and can be pictured as a cubic

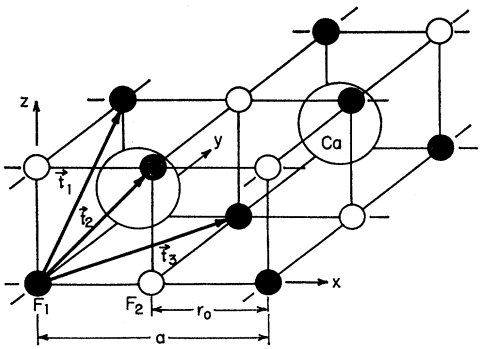

FIG. 3. Crystal structure of the (fcc) CaF_2 lattice, with the primitive translation vectors $\mathbf{t}_1$, $\mathbf{t}_2$, $\mathbf{t}_3$ shown. The primitive cell contains three basis atoms, Ca, F_1, and F_2, labeled $\kappa=1,2,3$.

[56] A. A. Maradudin, E. W. Montroll, and G. H. Weiss, in *Solid State Physics*, edited by F. Seitz and D. Turnbull (Academic Press Inc., New York, 1963), Suppl. 3.

[57] M. Born and K. Huang, *Dynamical Theory of Crystal Lattices* (Oxford University Press, New York, 1966).

[58] S. Ganesan and R. Srinivasan, Can. J. Phys. **40**, 74 (1962); **40**, 91 (1962).

lattice of fluorine ions, with metal ++ ions in every other body-centered position. The present model includes short-range forces between nearest-neighbor fluorines, nearest-neighbor calciums, and between a given calcium and its nearest-neighbor fluorines. Symmetry techniques can be used to show that the most general forms of the force constant matrices are

$$\Phi^0(\tfrac{1}{2}r_0,\tfrac{1}{2}r_0,\tfrac{1}{2}r_0;\ \mathrm{Ca,F}) = -\begin{pmatrix}\alpha_1 & \beta_1 & \beta_1\\ \beta_1 & \alpha_1 & \beta_1\\ \beta_1 & \beta_1 & \alpha_1\end{pmatrix},$$

$$\Phi^0(r_0,r_0,0;\ \mathrm{Ca,Ca}) = -\begin{pmatrix}\beta_2 & \gamma_2 & 0\\ \gamma_2 & \beta_2 & 0\\ 0 & 0 & \alpha_2\end{pmatrix}, \qquad (7)$$

$$\Phi^0(r_0,0,0;\ \mathrm{F,F}) = -\begin{pmatrix}\alpha_3 & 0 & 0\\ 0 & \beta_3 & 0\\ 0 & 0 & \beta_3\end{pmatrix},$$

with all of the other tensors obtained from appropriate rotation operations. (r_0 is the F-F separation, which is half of the "lattice constant.") The "self-" force constant matrices $\Phi^0(0,0,0;\ \mathrm{Ca,Ca})$ and $\Phi^0(0,0,0;\ \mathrm{F,F})$ can be calculated from the condition

$$\sum_{l'\kappa'} \Phi(l\kappa,l'\kappa') = 0 \qquad (8)$$

that results from invariance of the lattice under a rigid-body translation, and are given by

$$\begin{aligned}\Phi^0(0,0,0;\ \mathrm{Ca,Ca}) &= 4(2\alpha_1+2\beta_2+\alpha_2)\mathbf{1},\\ \Phi^0(0,0,0;\ \mathrm{F,F}) &= 2(\alpha_3+2\beta_3+2\alpha_1)\mathbf{1}.\end{aligned} \qquad (9)$$

The short-range force contributions to the Fourier-transformed dynamical matrix [Eq. (5)] become

$$\begin{aligned}
D_{xx}{}^{sr}(\mathbf{k}|1,1) &= (4/m_{\mathrm{Ca}})[2\alpha_1+\beta_2(2-\cos k_x\cos k_y\\
&\quad -\cos k_x\cos k_z)+\alpha_2(1-\cos k_y\cos k_z)],\\
D_{xy}{}^{sr}(\mathbf{k}|1,1) &= (4/m_{\mathrm{Ca}})\gamma_2\sin k_x\sin k_y,\\
D_{xx}{}^{sr}(\mathbf{k}|1,2) &= -4\alpha_1(m_{\mathrm{Ca}}m_{\mathrm{F}})^{-1/2}[\cos\tfrac{1}{2}k_x\cos\tfrac{1}{2}k_y\cos\tfrac{1}{2}k_z\\
&\quad +i\sin\tfrac{1}{2}k_x\sin\tfrac{1}{2}k_y\sin\tfrac{1}{2}k_z],\\
D_{xy}{}^{sr}(\mathbf{k}|1,2) &= 4\beta_1(m_{\mathrm{Ca}}m_{\mathrm{F}})^{-1/2}[\sin\tfrac{1}{2}k_x\sin\tfrac{1}{2}k_y\cos\tfrac{1}{2}k_z\\
&\quad +i\sin\tfrac{1}{2}k_z\cos\tfrac{1}{2}k_x\cos\tfrac{1}{2}k_y],\\
D_{xx}{}^{sr}(\mathbf{k}|2,3) &= -(2/m_{\mathrm{F}})[\alpha_3\cos k_x+\beta_3(\cos k_y+\cos k_z)],\\
D_{xy}{}^{sr}(\mathbf{k}|2,3) &= 0,\\
D_{\alpha\beta}{}^{sr}(\mathbf{k}|1,3) &= D_{\alpha\beta}{}^{sr}(\mathbf{k}|1,2)^*,\\
D_{\alpha\beta}{}^{sr}(\mathbf{k}|2,2) &= D_{\alpha\beta}{}^{sr}(\mathbf{k}|3,3) = (2/m_{\mathrm{F}})(\alpha_3+2\beta_3+2\alpha_1),
\end{aligned} \qquad (10)$$

with all other elements determined by cyclic permutation of x, y, and z. (The components of the $\mathbf{k}$ vector are expressed in dimensionless units for which r_0 is taken to be unity.) The three basis atoms of the unit cell, Ca, F_1, and F_2 of Fig. 3, are denoted by 1, 2, and 3, respectively, in Eqs. (10).

In the harmonic approximation, the quadratic truncation of the $(1/r)$ Coulomb forces leads to a sum of dipole-dipole interactions, distributed over the entire lattice. In the present model, the charges on the rigid nonpolarizable ions are assumed to be $+2Ze$ for calcium, and $-Ze$ for fluorine, where Ze is an effective charge which (along with the other constants α_1, α_2, α_3, β_2, β_3, and γ_2) will be determined from experimentally observed parameters. Since the ions are assumed to be rigid and nonpolarizable, the dipole moments arise purely from mechanical displacements from equilibrium. Thus, if the Coulomb energy is expressed as a quadratic form, the electrostatic contribution to the force constants becomes

$$\begin{aligned}\Phi^{\mathrm{Coul}}(i,j) &= -\frac{q_iq_j}{R_{ij}{}^3}\left\{3\frac{\mathbf{R}_{ij}\mathbf{R}_{ij}}{R_{ij}{}^2}-\mathbf{1}\right\}, \quad (i\neq j)\\ \Phi^{\mathrm{Coul}}(i,j) &= 0, \quad (i=j)\end{aligned} \qquad (11)$$

where i and j refer to ion sites, q_i q_j to the effective charges, and $\mathbf{R}_{ij}=\mathbf{R}_i-\mathbf{R}_j$ is the equilibrium separation between sites i, j. The Coulomb contribution to the Fourier transformed dynamical matrix can then be written

$$\mathbf{D}^{\mathrm{Coul}}(\mathbf{k}|\kappa\kappa') = -\frac{q_\kappa q_{\kappa'}}{(M_\kappa M_{\kappa'})^{1/2}}\mathbf{S}(\mathbf{k},\mathbf{r}_{\kappa\kappa'}), \qquad (12)$$

where

$$\mathbf{S}(\mathbf{k},\mathbf{r}_{\kappa\kappa'}) = \sum_l{}' \frac{e^{-i\mathbf{k}\cdot(\mathbf{R}_l+\mathbf{r}_{\kappa\kappa'})}}{|\mathbf{R}_l+\mathbf{r}_{\kappa\kappa'}|^3} \times\left\{3\frac{(\mathbf{R}_l+\mathbf{r}_{\kappa\kappa'})(\mathbf{R}_l+\mathbf{r}_{\kappa\kappa'})}{|\mathbf{R}_l+\mathbf{r}_{\kappa\kappa'}|^2}-\mathbf{1}\right\}. \qquad (13)$$

The vector $\mathbf{r}_{\kappa\kappa'}=\mathbf{R}_\kappa-\mathbf{R}_{\kappa'}$ is the relative displacement of two ions κ, κ' within a unit cell, and the prime on the sum means that terms for which $(\mathbf{R}_l+\mathbf{r}_{\kappa\kappa'})=0$ are to be omitted. (Clearly, no primitive translation vector $\mathbf{R}_l$ can make $(\mathbf{R}_l+\mathbf{r}_{\kappa\kappa'})=0$ unless $\kappa=\kappa'$, so the prime on the sum refers only to that case.) The summand of (13) falls off as $1/R_l{}^3$ at large distances, but since the area of a spherical shell goes as $R_l{}^2$, the sum falls off only $\sim 1/R_l$. However, the convergence is assisted by the phase factor, $\exp[-i\mathbf{k}\cdot(\mathbf{R}_l+\mathbf{r}_{\kappa\kappa'})]$, which oscillates rapidly as $\mathbf{R}_l$ increases, and by the dyadic expression in curly brackets (an angular factor which has Y_{2m} symmetry) whose contribution over a large sphere tends to average to zero. The convergence of (13) is extremely slow, and as $\mathbf{k}\to 0$, the sum is only conditionally convergent, and depends (in a *limiting way*) on the *direction of approach* to the origin. This fact leads to the well-known phenomenon of splitting the degeneracy between the transverse and longitudinal F_{1u} modes in CaF_2.

In order to evaluate the Coulomb contribution (12) to the dynamical matrix $\mathbf{D}^0(\mathbf{k}|\kappa\kappa')$, it is advantageous to use techniques formulated by Nijboer and De Wette[59,60] for a general class of lattice sums. Using

[59] B. R. A. Nijboer and F. W. De Wette, Physica **23**, 309 (1957); **24**, 422 (1958); **24**, 1105 (1958).

[60] F. W. De Wette, Physica **25**, 1225 (1959); Phys. Rev. **123**, 103 (1961).

those methods, it is possible to show that the dyadic lattice sum $\mathbf{S}(\mathbf{k},\mathbf{r}_{\kappa\kappa'})$ can be expressed as

$$\mathbf{S}(\mathbf{k},\mathbf{r}_{\kappa\kappa'})=\sum_l{}' \frac{e^{-i\mathbf{k}\cdot(\mathbf{R}_l+\mathbf{r}_{\kappa\kappa'})}}{|\mathbf{R}_l+\mathbf{r}_{\kappa\kappa'}|^3}\left\{3\frac{(\mathbf{R}_l+\mathbf{r}_{\kappa\kappa'})(\mathbf{R}_l+\mathbf{r}_{\kappa\kappa'})}{|\mathbf{R}_l+\mathbf{r}_{\kappa\kappa'}|^2}-1\right\}$$
$$\times[\mathrm{erfc}(\sqrt{\alpha}|\mathbf{R}_l+\mathbf{r}_{\kappa\kappa'}|)+2|\mathbf{R}_l+\mathbf{r}_{\kappa\kappa'}|(\alpha/\pi)^{1/2}$$
$$\times e^{-\alpha|\mathbf{R}_l+\mathbf{r}_{\kappa\kappa'}|^2}(1+\tfrac{2}{3}\alpha|\mathbf{R}_l+\mathbf{r}_{\kappa\kappa'}|^2)]$$
$$-\frac{4\pi}{3v_a}\sum_\lambda e^{-i\mathbf{h}_\lambda\cdot\mathbf{r}_{\kappa\kappa'}-|\mathbf{h}_\lambda-\mathbf{k}|^2/4\alpha}\left\{3\frac{(\mathbf{h}_\lambda-\mathbf{k})(\mathbf{h}_\lambda-\mathbf{k})}{|\mathbf{h}_\lambda-\mathbf{k}|^2}-1\right\}, \tag{14}$$

where $v_a=2r_0^3$ is the volume of the primitive cell, α is an arbitrary constant, and $\mathbf{h}_\lambda$ are the reciprocal lattice vectors. $\mathbf{S}(\mathbf{k},\mathbf{r}_{\kappa\kappa'})$ can thus be decomposed into two sums, one over the real lattice, and the other over the reciprocal lattice, and both sums are rapidly converging. The constant α can be chosen conveniently to make the two series converge approximately equally rapidly ($\alpha=\frac{1}{2}\pi$ was used for the calculations). The Coulomb contribution (12) can be expressed completely in terms of three sums $\mathbf{S}(\mathbf{k},\mathbf{r}_{\kappa\kappa'})$ as

$$\mathbf{D}^{\mathrm{Coul}}(\mathbf{k}|1,1)=-\frac{4Z^2e^2}{m_{\mathrm{Ca}}}\mathbf{S}(\mathbf{k},[000]),$$
$$\mathbf{D}^{\mathrm{Coul}}(\mathbf{k}|2,2)=-\frac{Z^2e^2}{m_{\mathrm{F}}}\mathbf{S}(\mathbf{k},[000])=\mathbf{D}^{\mathrm{Coul}}(\mathbf{k}|3,3),$$
$$\mathbf{D}^{\mathrm{Coul}}(\mathbf{k}|1,2)=2\frac{Z^2e^2}{(m_{\mathrm{Ca}}m_{\mathrm{F}})^{1/2}}\mathbf{S}(\mathbf{k},[\tfrac{1}{2}\tfrac{1}{2}\tfrac{1}{2}])=\mathbf{D}^{\mathrm{Coul}}(\mathbf{k}|2,1)^*, \tag{15}$$
$$\mathbf{D}^{\mathrm{Coul}}(\mathbf{k}|1,3)=\mathbf{D}^{\mathrm{Coul}}(\mathbf{k}|3,1)^*=\mathbf{D}^{\mathrm{Coul}}(\mathbf{k}|2,1),$$
$$\mathbf{D}^{\mathrm{Coul}}(\mathbf{k}|3,2)=-\frac{Z^2e^2}{m_{\mathrm{F}}}\mathbf{S}(\mathbf{k},[100])=\mathbf{D}^{\mathrm{Coul}}(\mathbf{k}|2,3)^*,$$

TABLE I. Experimental constants for CaF_2 (at $\sim$4°K), with the resulting rigid-ion model parameters. The force constants α_1, β_1, ... are expressed in dimensionless form as multiples of e^2/r_0^3 ($=1.14\times10^4$ dyn/cm in cgs units).

ω_R (cm^{-1})	326	Z^2	0.609
ω_{TO} (cm^{-1})	267[a]	α_1	1.537
ω_{LO} (cm^{-1})	472[a]	β_1	2.707
ϵ_0	6.38[a]	β_2	0.315
ϵ_∞	2.047[a]	γ_2	0.274
C_{11} (dyn/cm^2)	17.4×10^{11} [b]	α_3	1.079
C_{12} (dyn/cm^2)	5.6×10^{11} [b]		
C_{44} (dyn/cm^2)	3.59×10^{11} [b]		
r_0 (Å)	2.725		

[a] Reference 70.
[b] D. R. Huffman and M. H. Norwood, Phys. Rev. **117**, 709 (1960).

and the complete dynamical matrix $\mathbf{D}^0(\mathbf{k}|\kappa\kappa')=\mathbf{D}^{sr}(\mathbf{k}|\kappa\kappa')+\mathbf{D}^{\mathrm{Coul}}(\mathbf{k}|\kappa\kappa')$ can be used in conjunction with (6) to obtain the phonon eigenfrequencies $\omega_{\mathbf{k}\sigma}$ and eigenvectors $w_\alpha(\kappa|\mathbf{k}\sigma)$ for the fluorite lattice.

It is instructive to examine the $\mathbf{k}=0$ modes in more detail. Using the standard techniques of group theory, it can be shown that the symmetry of the long-wavelength modes is given by $\Gamma(\mathbf{k}=0)=F_{2g}+2F_{1u}$. One of these F_{1u} representations corresponds to the (three) acoustic phonon branches, while the other six degrees of freedom correspond to optic modes. The (triply degenerate) F_{2g} mode is Raman active, and the infrared active F_{1u} mode is split into longitudinal and transverse branches, as we shall show below. This phenomenon is connected with the macroscopic polarization field which accompanies a polar vibrational mode, and arises because of the long-range Coulomb interactions.[57] It is easy to show that, for the even F_{2g} mode, the calciums remain stationary, while the two fluorine sublattices vibrate against each other. For the odd F_{1u} optic mode, the fluorines all have the same displacement, and that of the calcium can be obtained by requiring the center of mass to be stationary in such a mode. The (unnormalized) mode vectors at $\mathbf{k}=0$ are

$$\mathbf{w}=\begin{array}{r|ccc|ccc|ccc}
 & & & & & & & & & \\
x & 0 & 0 & 0 & -2/\sqrt{m_{\mathrm{Ca}}} & 0 & 0 & \sqrt{m_{\mathrm{Ca}}} & 0 & 0 \\
(\mathrm{Ca})y & 0 & 0 & 0 & 0 & -2/\sqrt{m_{\mathrm{Ca}}} & 0 & 0 & \sqrt{m_{\mathrm{Ca}}} & 0 \\
z & 0 & 0 & 0 & 0 & 0 & -2/\sqrt{m_{\mathrm{Ca}}} & 0 & 0 & \sqrt{m_{\mathrm{Ca}}} \\
x & 1 & 0 & 0 & 1/\sqrt{M_{\mathrm{F}}} & 0 & 0 & \sqrt{m_{\mathrm{F}}} & 0 & 0 \\
(\mathrm{F}_1)y & 0 & 1 & 0 & 0 & 1/\sqrt{m_{\mathrm{F}}} & 0 & 0 & \sqrt{m_{\mathrm{F}}} & 0 \\
z & 0 & 0 & 1 & 0 & 0 & 1/\sqrt{m_{\mathrm{F}}} & 0 & 0 & \sqrt{m_{\mathrm{F}}} \\
x & -1 & 0 & 0 & 1/\sqrt{m_{\mathrm{F}}} & 0 & 0 & \sqrt{m_{\mathrm{F}}} & 0 & 0 \\
(\mathrm{F}_2)y & 0 & -1 & 0 & 0 & 1/\sqrt{m_{\mathrm{F}}} & 0 & 0 & \sqrt{m_{\mathrm{F}}} & 0 \\
z & 0 & 0 & -1 & 0 & 0 & 1/\sqrt{m_{\mathrm{F}}} & 0 & 0 & \sqrt{m_{\mathrm{F}}} \\
 & & F_{2g} & & & F_{1u}\text{ optic mode} & & & F_{1u}\text{ acoustic mode} &
\end{array}. \tag{16}$$

If the term in (14) for which $\lambda=(0,0,0)$ is split off, the two remaining sums are absolutely (and rapidly) convergent, and as $\mathbf{k}\to0$, the value of each will approach zero. (This is a consequence of the fact that both sums will contain an angular factor Y_{2m} symmetry, and there exists no linear combination of the spherical harmonics

Y_{2m} that has *cubic* symmetry.) Thus, as $\mathbf{k}\rightarrow 0$, only the $\lambda=(0,0,0)$ term will remain, and

$$\lim_{\mathbf{k}\rightarrow 0}\mathbf{S}(\mathbf{k},\mathbf{r}_{\kappa\kappa'})=-(4\pi/3v_a)\left[3\frac{\mathbf{kk}}{k^2}-\mathbf{1}\right]. \quad (17)$$

This dyad clearly depends upon the direction of approach as we take the limit $\mathbf{k}\rightarrow 0$, but it is independent of $\mathbf{r}_{\kappa\kappa'}$. The dyad $(3\mathbf{kk}/k^2-\mathbf{1})$ can be taken to define a set of axes with one longitudinal vector parallel to $\mathbf{k}$, and two (arbitrarily selected) transverse vectors perpendicular to $\mathbf{k}$. In that cartesian system, the dyad is diagonal, with eigenvalues, respectively, 2, -1, -1. It is easy to show, from Eqs. (10) and (15)–(17) that the limiting $\mathbf{k}\rightarrow 0$ frequencies are given by

$$\omega_R^2=(4/m_F)(\alpha_1+\alpha_3+2\beta_3), \quad (18a)$$

$$\omega_{TO}^2=2\left[\frac{1}{m_F}+\frac{2}{m_{Ca}}\right]\left(2\alpha_1-\frac{4\pi}{3v_a}Z^2e^2\right), \quad (18b)$$

$$\omega_{LO}^2=2\left[\frac{1}{m_F}+\frac{2}{m_{Ca}}\right]\left(2\alpha_1+\frac{8\pi}{3v_a}Z^2e^2\right), \quad (18c)$$

where ω_R is the frequency of the F_{2g} Raman mode, and ω_{TO} and ω_{LO} are the transverse and longitudinal F_{1u} frequencies. These relations can be used to help determine the parameters of the rigid-ion model; three other relations are supplied by the expressions[58] for the first-order elastic constants,

$$C_{11}=\frac{1}{r_0}\left[\alpha_1+2\beta_2+\alpha_3+3\frac{Z^2e^2}{v_a}\right], \quad (19a)$$

$$C_{12}=\frac{1}{r_0}\left[2\beta_1-2\gamma_2-\alpha_1-2\alpha_2-\beta_2-\beta_3-\frac{11}{2}\frac{Z^2e^2}{v_a}\right], \quad (19b)$$

$$C_{44}=\frac{1}{r_0}\left[\alpha_1+2\alpha_2+\beta_2+\beta_3-3\frac{Z^2e^2}{v_a}-\frac{(-\beta_1+5Z^2e^2/v_a)^2}{\alpha_1+\alpha_3+2\beta_3}\right]. \quad (19c)$$

Following Ganesan and Srinivasan,[58] we can reduce the number of force constants from eight to six by making the assumption that α_2 and β_3, which measure forces at right angles to the relative displacement of two atoms, are zero. The six remaining constants, α_1, β_1, β_2, γ_2, α_3, and Z^2 can then be determined from Eqs. (18) and (19). The ω_{LO} frequency is usually obtained from the experimentally measured TO frequency using the Lyddane-Sachs-Teller formula, $\omega_{LO}=\omega_{TO}(\epsilon_0/\epsilon_\infty)^{1/2}$. Using the experimental constants given in Table I, the phonon density of states, and dispersion curves for the [100], [110], and [111] directions have been calculated[61] for CaF_2 (at $\sim$4°K), and are shown in Fig. 4.

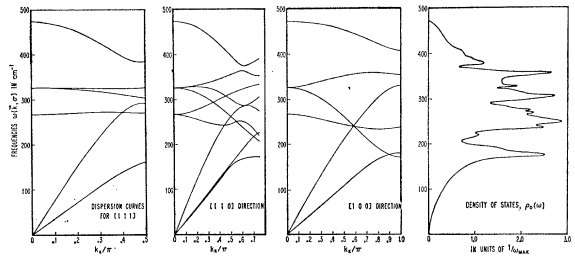

FIG. 4. Calculated phonon density of states and dispersion curves in certain directions of high symmetry for CaF_2 (based on the rigid-ion model).

B. Green's-Function Formalism

The (retarded) Green's function (at temperature T) for two Heisenberg operators $A(t)$ and $B(t')$ is defined by[31–38]

$$G^{AB}(t-t')=(1/i)\theta(t-t')\langle[A(t),B(t')]\rangle_T, \quad (20)$$

where $\theta(t)$ is the unit step function, defined by $\theta(t)=0$ for $t<0$, and $\theta(t)=1$ for $t>0$. The brackets $\langle\ \rangle_T$ represent an average over a thermodynamic ensemble defined by a density matrix $\exp[-\beta\mathcal{H}]$, where $\beta=1/kT$. This Green's function can be used to express, to lowest order, the *driven response* of a system in thermodynamic equilibrium at temperature T, to an externally applied field. If the unperturbed system is defined by the Hamiltonian $\mathcal{H}$, and an external perturbation is applied which couples a driving force $F(t)$ to some operator B, such that the new Hamiltonian is given by $H=\mathcal{H}+B\cdot F(t)$, then the response for an operator A is given by

$$\langle A\rangle_T(t)=\frac{1}{i}\int_{-\infty}^{t}dt'\,\langle[A(t),B(t')]\rangle_T F(t')=\int_{-\infty}^{\infty}dt'G^{AB}(t-t')F(t') \quad (21)$$

to lowest order in F. For the case of an external field of frequency ω, given by (the real part of) $F_\omega(t)=F_0\times\exp(-i\omega t+\epsilon t)$, the response becomes $\langle A\rangle_T(t)=\chi^{AB}(\omega)\times F_\omega(t)$, where the *linear susceptibility* $\chi^{AB}(\omega)$ can be expressed in terms of the Fourier transform

$$G^{AB}(z)=\int_{-\infty}^{\infty}dt\,e^{izt}G^{AB}(t) \quad (22)$$

by $\chi^{AB}(\omega)=G^{AB}(\omega+i\epsilon)$. Frequently, the Fourier transform of certain thermally averaged correlation functions of the form $R^{AB}(t-t')=\langle A(t)B(t')\rangle_T$ appears in the treatment of physically observable quantities. It can be shown[38] that such a correlation function has a spectral

[61] Following Ref. 58, the force constant β_1 is modified in the $\omega_{k\sigma}$ calculations by giving it a $\mathbf{k}$ dependence: $\beta_1\rightarrow\beta_1(1-0.3k^2/\pi^2)$.

density given by

$$\int_{-\infty}^{\infty} dt\, e^{i\omega t}\langle A(t)B(0)\rangle_T = i[1+n(\omega)] \times \lim_{\epsilon\to 0^+}[G^{AB}(\omega+i\epsilon)-G^{AB}(\omega-i\epsilon)], \quad (23)$$

where $n(\omega)=[e^{\beta\omega}-1]^{-1}$ is the Bose distribution function. The Green's function that is useful for the vibrational problem is the displacement-displacement phonon Green's function,

$$G_{\alpha\beta}(l\kappa,l'\kappa';t)=(1/i)\theta(t)\langle[u_\alpha(l\kappa,t),u_\beta(l'\kappa',0)]\rangle_T, \quad (24)$$

which satisfies an equation of motion, in matrix notation,

$$(\mathbf{M}d^2/dt^2+\mathbf{\Phi})\mathbf{G}(t)=-\delta(t)\mathbf{1}. \quad (25)$$

Where it exists, the Fourier transform (22) for (24) is given by $\mathbf{G}(\omega)^{-1}=\mathbf{M}\omega^2-\mathbf{\Phi}$. The eigenfrequencies ω_s for the normal modes of vibration are determined from the secular equation $\det(\mathbf{M}\omega^2-\mathbf{\Phi})=0$, and thus appear (for a finite crystal) as simple poles of $\mathbf{G}$ along the real axis in the (complex) frequency plane. For the perfect lattice, the Green's function $\mathbf{G}^0(z)$ can be expressed in terms of the dynamical matrix $\mathbf{D}^0$ as

$$\mathbf{G}^0(z)=\mathbf{M}_0^{-1/2}\frac{1}{z^2-\mathbf{D}^0}\mathbf{M}_0^{-1/2} =\mathbf{M}_0^{-1/2}\sum_{\mathbf{k}\sigma}\frac{|\mathbf{k}\sigma\rangle\langle\mathbf{k}\sigma|}{z^2-\omega_{\mathbf{k}\sigma}^2}\mathbf{M}_0^{-1/2}. \quad (26)$$

Then, using (4), $G_{\alpha\beta}^0(l\kappa,l'\kappa';z)=\langle l\kappa\alpha|\mathbf{G}^0(z)|l'\kappa'\beta\rangle$ can be written in spectral form as

$$G_{\alpha\beta}^0(l\kappa,l'\kappa';z)=\frac{1}{NM_\kappa^{1/2}}\sum_{\mathbf{k}\sigma}e^{i\mathbf{k}\cdot(\mathbf{R}_{l\kappa}-\mathbf{R}_{l'\kappa'})} \times\frac{w_\alpha(\kappa|\mathbf{k}\sigma)w_\beta^*(\kappa'|\mathbf{k}\sigma)}{z^2-\omega_{\mathbf{k}\sigma}^2}\frac{1}{M_{\kappa'}^{1/2}}. \quad (27)$$

For a finite lattice, the Green's function $\mathbf{G}^0(z)$ has poles along the real axis which become densely spaced as $N\to\infty$, and is analytic in the upper half-plane. In an infinite crystal, $\mathbf{G}^0(z)$ will have branch cuts along the portions of the real axis corresponding to the (positive and negative) frequency bands of the crystal. Specifically, if $\omega(>0)$ is *in* one of the phonon vibrational bands of the perfect lattice, then the Green's function $\mathbf{G}^0(z)$ will exhibit a jump discontinuity as z crosses the real axis from $\omega+i\epsilon$ to $\omega-i\epsilon$:

$$\mathbf{G}^0(\omega\pm i\epsilon)=\mathbf{H}^{(1)}(\omega)\mp i\mathbf{H}^{(2)}(\omega), \quad (28)$$

where the matrix $\mathbf{H}^{(2)}(\omega)$ is given by

$$\mathbf{H}^{(2)}(\omega)=\pi\mathbf{M}_0^{-1/2}\sum_{\mathbf{k}\sigma}|\mathbf{k}\sigma\rangle\delta(\omega^2-\omega_{\mathbf{k}\sigma}^2)\langle\mathbf{k}\sigma|\mathbf{M}_0^{-1/2}. \quad (29)$$

The real part $\mathbf{H}^{(1)}(\omega)$ is given by a Hilbert transform,

$$\mathbf{H}^{(1)}(\omega)=\frac{1}{\pi}\mathcal{P}\int d\omega'^2\frac{\mathbf{H}^{(2)}(\omega')}{\omega^2-\omega'^2}. \quad (30)$$

By means of the transformation function (4), the matrices $\mathbf{H}^{(1)}(\omega)$, $\mathbf{H}^{(2)}(\omega)$ can be expressed in the crystal lattice site representation $|l\kappa\alpha\rangle$; thus, for example,

$$H_{\alpha\beta}^{(2)}(l\kappa,l'\kappa';\omega)=\frac{\pi}{N(M_\kappa M_{\kappa'})^{1/2}}\sum_{\mathbf{k}\sigma}\delta(\omega^2-\omega_{\mathbf{k}\sigma}^2) \times e^{i\mathbf{k}\cdot(\mathbf{R}_{l\kappa}-\mathbf{R}_{l'\kappa'})}w_\alpha(\kappa|\mathbf{k}\sigma)w_\beta^*(\kappa'|\mathbf{k}\sigma). \quad (31)$$

Clearly, if ω lies outside of the phonon frequency band(s), the imaginary part $\mathbf{H}^{(2)}(\omega)$ of the Green's function $\mathbf{G}^0(\omega+i\epsilon)$ will vanish, since the δ functions can only make a contribution when ω is in one of the band(s). Equation (28) shows that the *sign* of the imaginary part of $\mathbf{G}^0(z)$ changes as the branch cut on the real axis is crossed.

The phonon Green's function $\mathbf{G}$ is useful for expressing many quantities of physical interest in lattice dynamical problems—e.g., density of states, Raman scattering intensity, dielectric susceptibility, etc. The formalism arises naturally as the most convenient mathematical framework for studying the perturbations due to impurities on the lattice dynamics of a pure crystal. Their usefulness for expressing concisely the coupling of an impurity site with the rest of the lattice, as well as their significance of representing the *response* of a lattice to an external (electromagnetic) field, makes them ideally suited for the study of the optical properties of crystals containing defects.

If an arbitrary configuration of (substitutional) impurities is introduced into a pure lattice, the perturbed Green's function is

$$\mathbf{G}(\omega)^{-1}=\mathbf{G}^0(\omega)^{-1}+\mathbf{V}, \quad (32)$$

where the "defect matrix" $\mathbf{V}$ is defined by

$$\mathbf{V}=(\mathbf{M}-\mathbf{M}_0)\omega^2-(\mathbf{\Phi}-\mathbf{\Phi}^0). \quad (33)$$

(It is always tacitly assumed that the subsitutional impurities do not distort the lattice; this is not strictly true, of course, but the assumption can be justified—or at least made plausible—by pointing out that lattice distortion effects will be implicitly incorporated in any realistic model of the host lattice and defect. For the *dynamical* properties of the crystal, the force constants are the fundamentally important quantities, and the lattice spacings do not appear explicitly in the results. Lattice distortion effects, along with possible changes in the form of the impurity interaction, are implicitly incorporated when the force constants are determined from experimentally measured quantities. This assumption is always made for this type of problem, since it is desirable to be able to continue to describe the lattice at equilibrium by the vectors $\mathbf{R}_{l\kappa}$ of the perfect lattice.)

In principle, Eq. (32) represents the solution for an arbitrary configuration of impurities, although for a general defect matrix $\mathbf{V}$, it has little practical usefulness for providing any explicit knowledge of the nature of the perturbed modes, or for changes in actual physical quantities. For a single, isolated, substitutional defect in an otherwise perfect lattice, it is possible to obtain several useful results from this formalism. If $\mathbf{v}_0$ is the defect matrix for a single impurity located at some site $i=(l_0,\kappa_0)$, then

$$\mathbf{G}_1(\omega)^{-1}=\mathbf{G}^0(\omega)^{-1}+\mathbf{v}_0, \tag{34}$$

and if the "defect subspace" (the total number of sites coupled by $\mathbf{v}_0$) is small, the techniques of matrix partition and the exploitation of group theory can be used to simplify the calculations.[33,40] The difficulty of carrying out numerical computations for an actual crystal lattice increases rapidly as the size of the impurity subspace increases, so it is often desirable, and usually necessary, to restrict the assumptions on force constant *changes*. In order to make a problem manageable, compromises have to be made that will provide a physically realistic model of the impurity and the host lattice, and simultaneously keep the defect subspace as small as possible. Since the use of Green's functions for such problems has been thoroughly discussed in the literature, particularly in several review articles, no further account is necessary here.

It was shown in an earlier publication[28] how it is possible to extend the single-impurity results to a random, disordered crystal, by means of a differential technique. The *average Green's function* $\langle\mathbf{G}(x,\omega)\rangle$ is given by

$$\langle\mathbf{G}(x,\omega)\rangle^{-1}=\mathbf{G}^0(\omega)^{-1}+\mathbf{F}(x,\omega), \tag{35}$$

where the *proper self-energy* (PSE) $\mathbf{F}(x)$ is assumed to be expandable in a power series:

$$\mathbf{F}(x,\omega)=x\mathbf{F}^{(1)}(\omega)+\tfrac{1}{2}x^2\mathbf{F}^{(2)}(\omega)+\cdots, \tag{36}$$

where

$$\mathbf{F}^{(1)}(\omega)=\sum_i \mathbf{v}_0(i)[\mathbf{1}+\mathbf{G}^0(\omega)\mathbf{v}_0(i)]^{-1}. \tag{37}$$

Analogous, but more complicated expressions hold for the higher-order terms. The brackets $\langle\ \rangle$ in (35) represent a "configurational average" over all possible arrangements of xN substitutional impurities (of the same type) in a perfect lattice described by $\mathbf{G}^0(\omega)$. To lowest order in the concentration,

$$\mathbf{M}_0^{1/2}\langle\mathbf{G}(x,\omega)\rangle\mathbf{M}_0^{1/2} =[\omega^2-\mathbf{D}^0+x\mathbf{M}_0^{-1/2}\mathbf{F}^{(1)}(\omega)\mathbf{M}_0^{-1/2}]^{-1}. \tag{38}$$

We shall later be interested in the function

$$\mathfrak{F}^{(1)}(\omega)=\mathbf{M}_0^{-1/2}\mathbf{F}^{(1)}(\omega)\mathbf{M}_0^{-1/2}, \tag{39}$$

which can be expressed in momentum space using (4) to obtain

$$\langle\mathbf{k}\sigma|\,\mathfrak{F}^{(1)}(\omega)\,|\mathbf{k}'\sigma'\rangle=\delta_{\mathbf{k}\mathbf{k}'}\mathfrak{F}^{(1)}(\mathbf{k},\omega)_{\sigma\sigma'}, \tag{40}$$

where

$$\mathfrak{F}^{(1)}(\mathbf{k},\omega)_{\sigma\sigma'}=\sum_{l\kappa\alpha,\,l'\kappa'\beta} e^{-i\mathbf{k}\cdot(\mathbf{R}l\kappa-\mathbf{R}l'\kappa')}w_\alpha^*(\kappa|\mathbf{k}\sigma)w_\beta(\kappa'|\mathbf{k}\sigma') \times M_\kappa^{-1/2}\langle l\kappa\alpha|\,\mathbf{v}_0[\mathbf{1}+\mathbf{g}^0(\omega)\mathbf{v}_0]^{-1}\,|l'\kappa'\beta\rangle M_{\kappa'}^{-1/2}. \tag{41}$$

$\mathbf{v}_0$ is the defect matrix for an impurity at some (arbitrary) origin in (41), so the summations over $(l\kappa\alpha)$ and $(l'\kappa'\beta)$ in (41) extend only over the defect subspace of a single impurity. The proper self-energy will be diagonal in $\mathbf{k}$, and since $\mathbf{G}^0(\omega)$ is diagonal in $\mathbf{k}$, the average Green's function $\langle\mathbf{G}(x,\omega)\rangle$ will also be diagonal. The mathematical process of averaging over all configurations has the important effect of restoring $\mathbf{k}$ as a good "quantum number," in a certain sense. $\langle\mathbf{G}(x,\omega)\rangle$ must have all of the space group symmetry of the empty lattice, and the fact that it is diagonal in $\mathbf{k}$ is an expression of the translational invariance that an "average crystal" would be expected to possess. This is not to say that there are eigenmodes of the perturbed system with well-defined momentum $\mathbf{k}$; the random, disordered crystal is defined by a configuration average over a large ensemble of systems, each of which is *not* periodic. An experiment which probes the crystal by exciting a disturbance of well-defined momentum $\mathbf{k}$ will, therefore, yield a *spread* in frequencies. Mathematically, this will be described by the imaginary part of the PSE.

C. Phonon Optical Properties

The phonon modes of a perfect lattice transform according to the irreducible representations of the crystal space group, and thus modes at $\mathbf{k}=0$ have the symmetry of the crystal point group. For a crystal which contains a center of inversion symmetry, Raman scattering and infrared absorption provide two complementary techniques for studying the long-wavelength optical modes. In this section, we shall show how these phenomena can be described using phonon Green's functions.

Raman scattering (RS) from lattice vibrations involves the creation (or destruction) of certain $\mathbf{k}\sim0$ phonons when light interacts with a crystal. An incident electromagnetic wave of frequency ω_i is coupled to the phonon modes of a crystal by means of the *electronic polarizability* $P_{\alpha\beta}$, which establishes an induced dipole moment

$$M_\alpha(l)=\sum_\beta P_{\alpha\beta}[\{\mathbf{u}_i(l)\};\omega_i]E_\beta(\omega_i)e^{-i\omega_i t}. \tag{42}$$

The prolarizability depends parametrically upon the instantaneous positions of the ions $\mathbf{u}_i(l)$, and the (inelastic) scattering mechanism is the *fluctuations* in $P_{\alpha\beta}$ that are induced by the vibrating lattice; the radiating dipole has a frequency ω_i that is modulated by lattice vibrational frequencies due to the intermediate coupling with the electronic structure. The description of Raman scattering in terms of the polarizability is

based on the early work of Born and Bradburn,[62] and has been expanded into a very useful formalism by Xinh,[63] which we shall follow here. A comprehensive review of many aspects of RS has also been given by Loudon.[64]

In the semiclassical approach to be followed here, the incident light field is regarded as a classical source, and the details of the electronic states of the system are lumped into certain phenomenological constants that characterize the polarizability $P_{\alpha\beta}$. It can be shown[57,63] that the intensity per unit solid angle for RS radiation at frequency $\omega_f=\omega_i+\omega$ is given by

$$I(\omega)=\frac{\omega_i^4}{2\pi c^3}\sum_{\alpha\beta\gamma\delta} n_\alpha n_\beta i_{\alpha\gamma,\beta\delta}(\omega)E_\gamma E_\delta^*, \tag{43}$$

where $\hat{n}$ is a unit polarization vector of the scattered radiation, and $\mathbf{E}$ is the (complex) amplitude of the electric field for the incident radiation. The scattering tensor $i_{\alpha\gamma,\beta\delta}(\omega)$ can be expressed as a Fourier transform of a correlation function for the electronic polarizability,

$$i_{\alpha\gamma,\beta\delta}(\omega)=\frac{1}{2\pi}\int_{-\infty}^{\infty} dt\, e^{i\omega t}\langle P_{\beta\delta}(t)P_{\alpha\gamma}^*(0)\rangle_T, \tag{44}$$

where $P_{\alpha\beta}(t)$ is a Heisenberg operator. If $P_{\alpha\beta}(t)$ is expanded in terms of the nuclear displacements

$$P_{\alpha\beta}(t)=P_{\alpha\beta}+\sum_{l\kappa\mu} P_{\alpha\beta,\mu}(l\kappa)u_\mu(l\kappa,t)+\cdots \tag{45}$$

and substituted into (44), the first term of (45) will contribute to Rayleigh scattering, the second term to first-order (one-phonon) RS, the next to second-order RS, and so on. For first-order RS,

$$i_{\alpha\gamma,\beta\delta}(\omega)=\sum_{l\kappa\mu,l'\kappa'\nu} P_{\alpha\gamma,\mu}(l\kappa)I_{\mu\nu}(l\kappa,l'\kappa';\omega)P_{\beta\delta,\nu}(l'\kappa'), \tag{46}$$

where

$$I_{\mu\nu}(l\kappa,l'\kappa';\omega)=\frac{1}{2\pi}\int_{-\infty}^{\infty} dt\, e^{i\omega t}\langle u_\mu(l\kappa,t)u_\nu(l'\kappa',0)\rangle_T. \tag{47}$$

The relation (23) can be used to express the Raman scattering intensity $I(\omega)$ in terms of the electronic coupling coefficients $P_{\alpha\beta,\mu}(l\kappa)$ and the phonon displacement-displacement Green's function (24):

$$I(\omega)\sim[n(\omega)+1]\sum_{l\kappa\mu,l'\kappa'\nu,\alpha\beta\gamma\delta} P_{\alpha\gamma,\mu}(l\kappa)\times\mathrm{Im}G_{\mu\nu}(l\kappa,l'\kappa';\omega+i\epsilon)P_{\beta\delta,\nu}(l'\kappa')\times n_\alpha n_\beta E_\gamma E_\delta^*. \tag{48}$$

This is a general result, valid for an arbitrary configuration of (substitutional) impurities in the lattice; if we define a (column) matrix $\mathbf{p}$, such that $\langle l\kappa\mu|\mathbf{p}=p_\mu(l\kappa)=\sum_{\alpha\beta} n_\alpha P_{\alpha\beta,\mu}(l\kappa)\cdot E_\beta$, Eq. (48) can be expressed in matrix notation as

$$I(\omega)\sim\mathbf{p}\,\mathrm{Im}\mathbf{G}(\omega+i\epsilon)\mathbf{p}. \tag{49}$$

For a perfect crystal, the coupling coefficients $P_{\alpha\beta,\mu}{}^0(l\kappa)$ are independent of the cell index l, and have symmetry properties determined by the group of operations that leave the crystal and the site κ invariant.[63] The symmetry of each site κ determines the *form* of the tensors $P_{\alpha\beta,\mu}{}^0(\kappa)$, and provides one point of view for obtaining the selection rules for the first-order Raman effect. The introduction of defects into a perfect crystal will, in general, alter these polarizability coefficients; if we define $\mathbf{p}=\mathbf{p}^0+\delta\mathbf{p}$, the Raman scattering intensity from a random, disordered crystal becomes

$$I(\omega)\sim\mathrm{Im}[\mathbf{p}^0\langle\mathbf{G}(\omega+i\epsilon)\rangle\mathbf{p}^0+\mathbf{p}^0\langle\mathbf{G}(\omega+i\epsilon)\delta\mathbf{p}\rangle+\langle\delta\mathbf{p}\mathbf{G}(\omega+i\epsilon)\rangle\mathbf{p}^0+\langle\delta\mathbf{p}\mathbf{G}(\omega+i\epsilon)\delta\mathbf{p}\rangle]. \tag{50}$$

Thus, in addition to perturbations in the lattice dynamics, the first-order RS also reflects changes in electronic properties. If the mixed crystal is formed from two similar isomorphs (such as the $Ca_{1-x}Sr_xF_2$ or $Ba_{1-x}Sr_xF_2$ systems), it may be reasonable to assume that the polarizability coefficients do not change significantly, and in that case, the dominant contribution to the spectrum would be given by the first term in (50),

$$I(\omega)\sim\mathbf{p}^0\langle\mathbf{G}(\omega+i\epsilon)\rangle\mathbf{p}^0. \tag{51}$$

For a host which has one first-order allowed Raman line (such as CaF_2), the coefficients $p_\mu{}^0(\kappa)$ have a structure that projects onto this ($\mathbf{k}=0$) Raman mode,

$$I(\omega)\sim\mathrm{Im}\langle\mathbf{k}=0,\sigma_R|\,\mathbf{M}_0{}^{1/2}\langle\mathbf{G}(\omega+i\epsilon)\rangle\times\mathbf{M}_0{}^{1/2}|\mathbf{k}=0,\sigma_R\rangle. \tag{52}$$

This can be shown by inserting a factor $\mathbf{M}_0{}^{-1/2}\cdot\mathbf{1}\cdot\mathbf{M}_0{}^{1/2}$ between $\mathbf{p}^0$ and $\langle\mathbf{G}\rangle$ and between $\langle\mathbf{G}\rangle$ and $\mathbf{p}^0$ in Eq. (51), with the following identity for the unit matrix:

$$\mathbf{1}=\frac{1}{\sqrt{N}}\sum_{l\kappa\mu\mathbf{k}\sigma}|l\kappa\mu\rangle e^{i\mathbf{k}\cdot\mathbf{R}_{l\kappa}}w_\mu(\kappa|\mathbf{k}\sigma)\langle\mathbf{k}\sigma|\,. \tag{53}$$

Since the coefficients $\langle l\kappa\mu|\,\mathbf{p}^0=p_\mu{}^0(\kappa)$ are independent of the cell index, the resulting sum over l that arises will produce a $\delta_{\mathbf{k},0}$ factor, and further simplification will lead to a sum

$$\sum_{\kappa\mu} p_\mu{}^0(\kappa)\frac{1}{\sqrt{M_\kappa}}w_\mu(\kappa|\mathbf{k}=0,\sigma)$$

that is nonvanishing only for the Raman-active mode $\sigma=\sigma_R$. Equation (52) shall be the basis for the numerical calculations for the $Ca_{1-x}Sr_xF_2$ system that are presented in Sec. IV.

If the impurities that are added to a pure lattice are radically different (in their electronic properties) from

[62] M. Born and M. Bradburn, Proc. Roy. Soc. (London) **A188**, 161 (1947).
[63] N. X. Xinh, Westinghouse Research Report No. 65-9F5-442-P8, 1965 (unpublished); J. Phys. (Paris) **28**, Suppl. 2, Cl-103 (1967).
[64] R. Loudon, Advan. Phys. **13**, 423 (1964).

the host atoms they replace—e.g., U centers in CaF_2—the RS may also exhibit contributions from the $\delta\mathbf{p}$ fluctuation terms in (50). The important thing to emphasize is that the spectrum of Raman scattering from phonons depends upon a combination of effects—lattice vibrational characteristics, and electronic polarizability. If the impurities differ mainly in mass or "spring-constant" characteristics, but are not very different in electronic structure, it is reasonable to assume that the polarizability coefficients will not change, or will change only slightly. In any case, some assumptions about the electronic coupling of defects (in addition to those about the mechanical, vibrational characteristics) must always be made if the Raman effect is to be used as a probe of the perturbed lattice dynamics of crystals containing impurities.

When far-infrared radiation impinges on a crystal, it interacts strongly with only those transverse optical phonon modes near $\mathbf{k}=0$ which possess an electric dipole moment. Stern[65] and Martin[66] have discussed the study of lattice vibrations by far-infrared spectroscopy, and Kubo[67] and many others[68,69] have used the Green's-function point of view to treat the complex dielectric constant $\epsilon(\omega)$, from which the absorption, reflectivity, etc. can be calculated. The review article by Maradudin[4] can be consulted for many references to work on impurity-induced infrared lattice absorption in crystals.

Although an accurate treatment of the interaction of light with the crystal lattice requires a redefinition of the normal modes of the total system of vibrations and radiation ("polaritons"), we can begin to discuss the problem in the limit that the electric dipole moment for these modes is vanishingly small. In such a process, the absorption of light energy is accompanied by the excitation of a phonon, but with no change in the electronic state of the crystal. The $\mathbf{k}\sim 0$ selection rule will be relaxed if impurities are introduced into the crystal and then light will be able to interact with other polar modes of the (imperfect) lattice. For a perfect crystal without phonon damping processes (i.e., in the harmonic approximation), the so-called reststrahlen bands are δ-function absorption peaks at the $\mathbf{k}\cong 0$ TO modes which have vectorlike symmetry.

Assume that a (long-wavelength) light field, turned on "adiabatically," interacts with the electric dipole moment $\mathbf{M}$ of a crystal lattice:

$$\mathcal{H}' = -\mathbf{M}\cdot\mathbf{E}\exp(-i\omega t+\epsilon t). \tag{54}$$

This perturbation is of the same form as that considered in Sec. III B, and leads to a response function $\chi_{\alpha\beta}(\omega)$ for $\langle M_\alpha\rangle_T(t)$ which can be expressed as the Fourier transform of the Green's function $G^{MM}(t)$ between two $\mathbf{M}$ operators:

$$\langle M_\alpha\rangle(t)=\sum_\beta \chi_{\alpha\beta}(\omega)E_\beta\exp(-i\omega t+\epsilon t), \tag{55}$$

where

$$\chi_{\alpha\beta}(\omega)=i\int_0^\infty dt\,\langle[M_\alpha(t),M_\beta(0)]\rangle_T\exp[i\omega t-\epsilon t]. \tag{56}$$

The electric dipole moment $\mathbf{M}$ can be expanded in terms of the ionic displacements,

$$M_\alpha(t)=\mathfrak{M}_\alpha+\sum_{l\kappa\mu}\mathfrak{M}_{\alpha,\mu}(l\kappa)u_\mu(l\kappa,t)+\cdots. \tag{57}$$

If it is assumed that there is no static polarization $\mathfrak{M}_\alpha$, and if only the first-order electric moment (linear term) is retained, then insertion of Eq. (57) into (56) will give the one-phonon absorption contribution to the far-infrared dielectric constant. The susceptibility becomes

$$\chi_{\alpha\beta}(\omega)=\sum_{l\kappa\mu,\,l'\kappa'\nu}\mathfrak{M}_{\alpha,\mu}(l\kappa)G_{\mu\nu}(l\kappa,l'\kappa';\omega+i\epsilon)\mathfrak{M}_{\beta,\nu}(l'\kappa'), \tag{58}$$

or, in matrix notation [and analogous to Eq. (50)],

$$\begin{aligned}\chi_{\alpha\beta}(\omega)=&\,\mathfrak{M}_\alpha{}^0\mathbf{G}(\omega+i\epsilon)\mathfrak{M}_\beta{}^0+\mathfrak{M}_\alpha{}^0\mathbf{G}(\omega+i\epsilon)\delta\mathfrak{M}_\beta\\&+\delta\mathfrak{M}_\alpha\mathbf{G}(\omega+i\epsilon)\mathfrak{M}_\beta{}^0+\delta\mathfrak{M}_\alpha\mathbf{G}(\omega+i\epsilon)\delta\mathfrak{M}_\beta,\end{aligned} \tag{59}$$

where we have defined a column, $\langle l\kappa\mu|\mathfrak{M}_\alpha=\mathfrak{M}_{\alpha,\mu}(l\kappa)$, and have expressed $\mathfrak{M}_\alpha+\mathfrak{M}_\alpha{}^0+\delta\mathfrak{M}_\alpha$, relating the perturbed crystal to the pure host. The first-order coefficients $\mathfrak{M}_{\alpha,\mu}(l\kappa)$ have the significance of representing an effective charge tensor, and just as for the force constants $\Phi_{\alpha\beta}(l\kappa,l'\kappa')$ and first-order electronic polarizability $P_{\alpha\beta,\mu}(l\kappa)$, they will satisfy certain symmetry conditions.[63] For the perfect crystal, the coefficients $\mathfrak{M}_{\alpha,\mu}{}^0(\kappa)$ are independent of the cell index, and (just as for the case of Raman scattering) the summations over l,l' in Eq. (58) will lead to a projection onto certain $\mathbf{k}\to 0$ modes. However, the limit as $\mathbf{k}\to 0$ of the phonon Green's function $\mathbf{G}$ is not uniquely defined for modes that have an electric dipole moment. This complication is related to the fact that the Coulomb contribution (15) to $\mathbf{D}^0(\mathbf{k})$ has a term [cf. Eq. (17)] that looks like $(3\mathbf{kk}/k^2-\mathbf{1})$ as $\mathbf{k}\to 0$; the limiting *singularities* are well defined, of course, but there will be a dependence upon the direction of approach. The origin of the splitting into longitudinal and transverse branches is the macroscopic electric field that is associated with the longitudinal wave.[57] The susceptibility $\chi_{\alpha\beta}(\mathbf{k}\to 0,\omega)$ can be expressed as[4]

$$\chi_{\alpha\beta}(\mathbf{k}\to 0,\omega)=\hat{k}_\alpha\hat{k}_\beta\chi^L(\omega)+[\delta_{\alpha\beta}-\hat{k}_\alpha\hat{k}_\beta]\chi^T(\omega). \tag{60}$$

There are, therefore, two scalar susceptibilities, $\chi^T(\omega)$ and $\chi^L(\omega)$, which measure the response of the lattice to transverse and longitudinal electromagnetic fields, respectively. It is the former quantity that is of in-

[65] F. Stern, in *Solid State Physics*, edited by F. Seitz and D. Turnbull (Academic Press Inc., New York, 1963), Vol. 15, p. 299.
[66] D. H. Martin, Advan. Phys. **14**, 39 (1964).
[67] R. Kubo, *Boulder Lectures in Theoretical Physics* (Academic Press Inc., New York, 1958), Vol. 1.
[68] H. Bilz, in *Phonons in Perfect Lattices and in Lattices with Point Imperfections*, edited by R. W. H. Stevenson (Plenum Press, Inc., New York, 1966).
[69] T. P. Martin, Phys. Rev. **160**, 686 (1967); **170**, 779 (1968).

terest for the optical properties, since the electric moment vector $\mathbf{M}$ is coupled to a transverse electric (radiation) field in Eq. (54). It is only the transverse optic phonon modes that can contribute to the lattice absorption, $\frac{1}{2}\langle \mathbf{E}\cdot d\mathbf{M}/dt\rangle = \omega\,\mathrm{Im}\chi^T(\omega)|\mathbf{E}(\omega)|^2$, and it will be only the transverse lattice susceptibility $\chi^T(\omega)$ that contributes to the optical dielectric constant $\epsilon(\omega)$. For a mixed crystal in which the first-order electric moment coefficients do not change appreciably from those of the pure host, the dominant contribution to the far infrared lattice susceptibility will come from the first term in Eq. (59), provided that the pure crystal has an infrared-active mode. (By using arguments similar to those invoked for RS above, we can show that $\mathfrak{M}_\alpha{}^0\mathbf{M}_0{}^{-1/2}$ projects onto $\mathbf{k}=0$ modes with polar vector symmetry.) If the effective-charge characteristics of the defects are significantly different from those of the pure host lattice, a more complicated situation results, and the $\delta\mathfrak{M}$ fluctuation terms in Eq. (59) must also be included. In general, it is very difficult to treat such problems if the concentration of impurities is not small, and, in fact, studies of impurity-induced RS of infrared absorption have generally been confined to systems in which the pure host lattice does not exhibit a first-order effect. Thus, if we adopt the assumptions above, the (transverse part) of the lattice susceptibility can be expressed as

$$\chi^T(\omega)\sim\langle \mathbf{k}=0,\mathrm{TO}|\,\mathbf{M}_0{}^{1/2}\langle\mathbf{G}(\omega+i\epsilon)\rangle \times\mathbf{M}_0{}^{1/2}|\mathbf{k}=0,\mathrm{TO}\rangle. \quad (61)$$

[This can be demonstrated by inserting a factor $\mathbf{M}_0{}^{-1/2}\cdot\mathbf{1}\cdot\mathbf{M}_0{}^{1/2}$ between $\mathfrak{M}^0$ and $\mathbf{G}$ and between $\mathbf{G}$ and $\mathfrak{M}^0$ in the first term of (59), and using the identity (53) for $\mathbf{1}$.] In addition to the TO optical-phonon contribution to the dielectric constant $\epsilon(\omega)$, there will also be a contribution from electronic absorption processes. In the far-infrared region, the frequency ω is so low that the latter processes contribute only a constant value, $\chi^e\sim(\epsilon_\infty-1)/4\pi$ to the total susceptibility (where ϵ_∞ is the high-frequency dielectric constant). Thus, if defects are added to a crystal with only one infrared-active mode, and if we assume that the first-order electric moment coefficients do not change, then for the disordered crystal

$$\epsilon(\omega)-\epsilon_\infty\sim K\langle\mathbf{k}=0,\mathrm{TO}|\,\mathbf{M}_0{}^{1/2}\langle\mathbf{G}(\omega+i\epsilon)\rangle\mathbf{M}_0{}^{1/2} \times|\mathbf{k}=0,\mathrm{TO}\rangle, \quad (62)$$

where the constant K is determined completely from parameters that characterize the pure host lattice. We can easily verify that this result holds for the perfect lattice by inserting the expression (26) for $\mathbf{G}^0(\omega+i\epsilon)$, which gives (for $\omega>0$)

$$\epsilon(\omega)-\epsilon_\infty\sim K\langle\mathbf{k}=0,\mathrm{TO}|\,(\omega^2-\mathbf{D}^0+i\epsilon)^{-1} \times|\mathbf{k}=0,\mathrm{TO}\rangle. \quad (63)$$

The constant K can be expressed as $K=-\omega_{\mathrm{TO}}{}^2(\epsilon_0-\epsilon_\infty)$, where $\epsilon_0=\epsilon(0)$ is the static dielectric constant, and we obtain the familiar result

$$\epsilon(\omega)=\epsilon_\infty-\frac{\epsilon_0-\epsilon_\infty}{\omega^2-\omega_{\mathrm{TO}}{}^2+i\epsilon}\omega_{\mathrm{TO}}{}^2. \quad (64)$$

Equation (62) for a mixed crystal becomes, finally,

$$\epsilon(\omega)/\epsilon_\infty-1=\left(1-\frac{\epsilon_0}{\epsilon_\infty}\right)\omega_{\mathrm{TO}}{}^2\langle\mathbf{k}=0,\mathrm{TO}|\,\mathbf{M}_0{}^{1/2} \times\langle\mathbf{G}(\omega+i\epsilon)\rangle\mathbf{M}_0{}^{1/2}|\mathbf{k}=0,\mathrm{TO}\rangle, \quad (65)$$

and will be the basis of the theoretical calculations of the infrared reflectivity spectra of the $Ca_{1-x}Sr_xF_2$ system, to be presented in Sec. IV.

IV. MIXED-FLUORITE SYSTEM, $Ca_{1-x}Sr_xF_2$

In addition to a physically realistic model for the pure CaF_2 lattice, a good model is needed to describe the effects of a substitutional Sr^{++} impurity. The calculation of the PSE, to lowest order in the concentration x, can be carried out for the mixed-fluorite system $Ca_{1-x}Sr_xF_2$ by using Eq. (41). In order to make the computational aspects of the problem manageable, assumptions have to be made on the force-constant changes (induced by a Sr^{++} impurity) that will keep the defect subspace as small as possible. In the model of the defect to be adopted here, we shall assume that the long-range Coulomb forces are not affected. The defect matrix $\mathbf{v}_0=(\mathbf{M}-\mathbf{M}_0)\omega^2-(\mathbf{\Phi}-\mathbf{\Phi}^0)$ shall be constructed from the following assumptions: (1) The mass of the $++$ metal ion changes (Sr^{++} replaces Ca^{++}); (2) the effective charge Ze does not change; and (3) all nearest-neighbor short-range interactions, except for that between $++$ ions, may change. These requirements lead to a defect space that contains nine atoms; it is an XY_8 complex, consisting of the $++$ impurity and its eight nearest fluorines, as shown in Fig. 5. The calculation of the first-order PSE from Eq. (41) requires the evaluation of $\mathbf{v}_0[\mathbf{1}+\mathbf{g}^0(\omega+i\epsilon)\mathbf{v}_0]^{-1}$, which is of order 27×27. Even with the present simple assumptions, the dimensionality of the impurity subspace is quite large, and without the simplifications that point symmetry can provide, the calculations would be a formidable task. The matrix $\mathbf{g}^0$ is the Green's function (imbedded) in

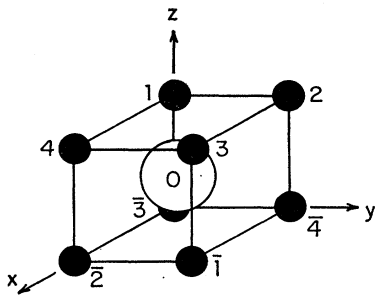

FIG. 5. XY_8 Impurity subspace.

that subspace, for the unperturbed lattice. Even though it is here confined to the defect subspace, $\mathbf{g}^0$ has the full symmetry of the perfect lattice—i.e., O_h point group symmetry, and also, translational symmetry. Instead of the 378 elements that a general (symmetric) 27×27 matrix possesses, $\mathbf{g}^0$ can be shown to have *only* 13 independent elements, as shown in Table II. (The notation 0, 1, 2,..., $\bar{1}$, $\bar{2}$,..., etc., refers to the site labels introduced in Fig. 5.) The real and imaginary parts of the thirteen independent elements A, B,..., U, V of the 27×27 matrix $\mathbf{g}^0(\omega+i\epsilon)$ in the XY_8 defect subspace have been computed numerically, as a function of frequency, and are shown in Fig. 9 in the Appendix.

The defect matrix $\mathbf{v}_0$, and also $\mathbf{v}_0[\mathbf{1}+\mathbf{g}^0(\omega+i\epsilon)\mathbf{v}_0]^{-1}$, has the site symmetry of the XY_8 complex. There will be one mass change, $(m_{\mathrm{Sr}}-m_{\mathrm{Ca}})$, and three force constant changes, $\delta\alpha_1$, $\delta\beta_1$, and $\delta\alpha_3$ involved in the defect matrix $\mathbf{v}_0$, whose form is given in Table III. The change in α_1 is calculated from Eqs. (18b) and (18c), using the (assumed unchanged) value of $Z^2=0.609$ and the value[70] of $\omega_{\mathrm{TO}}=225$ cm^{-1} for SrF_2 (at ~4°K); the change in β_1 is obtained from Eq. (19b) using the experimental value[71] of $C_{12}=4.75\times10^{11}$ dyn/cm^2 for SrF_2 (at ~4°K); and the change in α_3 comes from Eq. (18a) using the experimental value of $\omega_R=290$ cm^{-1} for SrF_2 (at ~4°K). The masses of Ca and Sr (relative to the fluorine mass) are, respectively, 2.109 and 4.612, so that the change is $\delta m=2.503$. Since every nearest-neighbor F-F pair shares the subspace for two possible impurity sites, the average α_3 force constant is used for two F^- ions located between a Sr^{++} defect and a Ca^{++} host atom. This is equivalent to associating a change of $\frac{1}{2}\alpha_3$ in the F-F matrix elements for the defect matrix $\mathbf{v}_0$ that describes a single Sr^{++} impurity. The "self-" force constant change in Table III were determined from the translation condition (8), which is valid for an arbitrary lattice.

Under each of the 48 operations of the O_h point group, a matrix $\mathbf{T}$ defined over the sites of the XY_8 impurity subspace will be subjected to a 27-dimensional similarity transformation $\mathcal{S}$: $\mathbf{T}\rightarrow\mathcal{S}\mathbf{T}\mathcal{S}^{-1}$. If $\mathbf{T}$ has the symmetry of the XY_8 defect "molecule," then it will be invariant under all of these similarity transformations, and $\mathbf{T}$ will commute with each of the 48 27-dimensional matrices $\mathcal{S}$. The 27-dimensional (reducible) representation formed by these similarity transformations can be shown to reduce to

$$\Gamma(XY_8)=A_{1g}+E_g+F_{1g}+2F_{2g}+A_{2u}+E_u+3F_{1u}+F_{2u}. \quad (66)$$

With some intuition, it is possible to construct 27-dimensional column vectors with the appropriate symmetries that can be used as "basis vectors" to reduce the matrix $\mathbf{T}$ into block form, corresponding to the decomposition (66) into orthogonal subspaces with A_{1g}, E_g, F_{1g},..., etc., symmetry. These (unnormalized) basis vectors are displayed in Table IV, and are, of course, not unique; all that is claimed for them is that they have the symmetry stated. They have been constructed so that the equivalent polarizations (e.g., in a three-dimensional representation such as F_{2g}) are orthogonal. However, since they were obtained purely by geometrical intuition, it will only be accidental if they diagonalize any given matrix $\mathbf{T}$ completely. All of the simplification that group theory can provide is contained in the decomposition (66), and since some representations (e.g., F_{2g} and F_{1u}) occur more than once, complete diagonalization in those subspaces cannot be accomplished by O_h symmetry considerations alone. Aside from the fact that there are three equivalent polarizations, the reduction of a matrix $\mathbf{T}$ with the symmetry of the XY_8 defect molecule will lead to (three) 2×2 F_{2g} blocks, and (three) 3×3 F_{1u} blocks. The diagonalization of these blocks will determine the linear combinations of F_{2g} and F_{1u} vectors (of Table IV) that diagonalize a given matrix $\mathbf{T}$ completely. The elements of the unperturbed Green's-function matrix $\mathbf{g}^0$ and of the defect matrix $\mathbf{v}_0$ can be calculated for each of the symmetry subspaces by using Tables II–IV. These calculations are rather tedious, and have been carried out for the F_{2g} and F_{1u} subspaces, with the results shown in Table V. These matrices (Table V) will be necessary later for the evaluation of $\mathbf{v}_0[\mathbf{1}+\mathbf{g}^0(\omega+i\epsilon)\mathbf{v}_0]^{-1}$ (which occurs in the first-order PSE) as a function of frequency in the F_{2g} and F_{1u} subspaces. (The constants p, q in Tables IV and V are related by $p=1/q$, but are otherwise arbitrary; it shall prove convenient for the later infrared calculations to choose $p=m_{\mathrm{Ca}}/m_{\mathrm{F}}$.)

A. Raman Scattering

It may be reasonable to assume that the formation of the mixed crystal $Ca_{1-x}Sr_xF_2$ from two similar isomorphs will not involve any appreciable changes in the $P_{\alpha\beta,\mu}{}^0(\kappa)$ coefficients that characterize the electronic polarizability of CaF_2. Evidence for this assumption could be taken to be the fact that significant changes in these quantities would most likely lead to induced scattering from impurity modes, other than the $\mathbf{k}\sim0$ excitation. Since this is contrary to our observations of a single peak which shifts linearly, and broadens with concentration, we shall assume that the dominant scattering mechanism comes from the first term in (50), which was expressed by Eq. (52). Using that result, we can write the scattering intensity as

$$I(\omega)\sim\mathrm{Im}[\omega^2-(\omega_R-i\Gamma_R/2)^2+i\epsilon+x\langle\sigma_R|\mathbf{M}_0^{-1/2}\mathbf{F}^{(1)}(\mathbf{k}=0,\omega+i\epsilon)\mathbf{M}_0^{-1/2}|\sigma_R\rangle]^{-1}, \quad (67)$$

to lowest order in the PSE. We have phenomenologically included a broadening to the $\mathbf{k}=0$ mode of pure CaF_2 by adding a term $-i\Gamma_R/2$ to ω_R, where Γ_R represents a full width. From Eqs. (16) and (41), it is evident that, as $\mathbf{k}\rightarrow0$ the PSE term in the denominator

[70] D. T. Bosomworth, Phys. Rev. **157**, 709 (1967).
[71] D. Gerlich, Phys. Rev. **136**, A1366 (1964).

TABLE II. The unperturbed phonon Green's-function matrix (which contains 13 independent functions $A, B, \ldots, U, V$) for the XY_8 impurity subspace shown in Fig. 5. The site labels $i, j = 0, 1, 2, \ldots$, etc., refer to the notation used in Fig. 5, and the matrix is partitioned so that each small 3×3 box represents a Cartesian dyad.

	0	1	2	3	4	$\bar{1}$	$\bar{2}$	$\bar{3}$	$\bar{4}$
0	A	$C\ D\ -D$	$C\ -D\ -D$	$C\ D\ D$	$C\ -D\ D$				
	A	$D\ C\ -D$	$-D\ C\ D$	$D\ C\ D$	$-D\ C\ -D$		$\mathbf{G}^0(0,\bar{i}) = \mathbf{G}^0(0,i)$		
	A	$-D\ -D\ C$	$-D\ D\ C$	$D\ D\ C$	$D\ -D\ C$				
1		B	$M\ \ H$	$P\ R\ S$	F	$U\ V\ -V$	$P\ -S\ -R$	$M\ -H$	$Q\ S\ -S$
		B	F	$R\ P\ S$	$M\ H$	$U\ -V$	$S\ Q\ -S$	$-H\ M$	$-S\ P\ -R$
		B	$H\ \ M$	$-S\ -S\ Q$	$H\ M$	U	$-R\ S\ P$	F	$S\ -R\ P$
2	$\mathbf{G}^0(i,0) = \mathbf{G}^0(0,\bar{i})^T$	B	F	$P\ -R\ S$		$U\ -V\ -V$	$Q\ -S\ -S$	$M\ H$	
		B	$M\ -H$	$-R\ P\ -S$		$U\ V$	$S\ P\ R$	$H\ M$	
		B	$-H\ M$	$-S\ S\ Q$		U	$S\ R\ P$		F
3		B	M	$-H$			$U\ V\ V$	$P\ -S\ R$	
		Symmetric block	B	F		Symmetric	$U\ V$	$S\ Q\ -S$	
			B	$-H$	M		U	$R\ S\ P$	
4		$\mathbf{G}^0(i,j) = \mathbf{G}^0(j,i)^T$	B	B		$\mathbf{G}^0(i,\bar{j}) = \mathbf{G}^0(j,\bar{i})^T$		$U\ -V\ V$	
				B				$U\ -V$	
					B				U
$\bar{1}$									
$\bar{2}$	$\mathbf{G}^0(\bar{i},0) = \mathbf{G}^0(0,\bar{i})^T$	Same as upper right block				Same as upper left block			
$\bar{3}$		$\mathbf{G}^0(\bar{i},j) = \mathbf{G}^0(i,\bar{j})$				$\mathbf{G}^0(\bar{i},\bar{j}) = \mathbf{G}^0(i,j)$			
$\bar{4}$									

TABLE III. The defect matrix $\mathbf{v}_0$ in the XY_8 impurity subspace. The site labels 0, 1, 2, ..., etc., refer to the notation used in Fig. 5.

	0	1	2	3	4	$\bar{1}$	$\bar{2}$	$\bar{3}$	$\bar{4}$
0	X_0	X_1	X_2	X_3	X_4	X_1	X_2	X_3	X_4
1	X_1	$-X_1-\frac{1}{2}\delta\alpha_3$	$\begin{matrix}0&&\\&\frac{1}{2}\delta\alpha_3&\\&&0\end{matrix}$		$\begin{matrix}\frac{1}{2}\delta\alpha_3&&\\&0&\\&&0\end{matrix}$			$\begin{matrix}0&&\\&0&\\&&\frac{1}{2}\delta\alpha_3\end{matrix}$	
2	X_2	$\begin{matrix}0&&\\&\frac{1}{2}\delta\alpha_3&\\&&0\end{matrix}$	$-X_2-\frac{1}{2}\delta\alpha_3$	$\begin{matrix}\frac{1}{2}\delta\alpha_3&&\\&0&\\&&0\end{matrix}$					$\begin{matrix}0&&\\&0&\\&&\frac{1}{2}\delta\alpha_3\end{matrix}$
3	X_3		$\begin{matrix}\frac{1}{2}\delta\alpha_3&&\\&0&\\&&0\end{matrix}$	$-X_3-\frac{1}{2}\delta\alpha_3$	$\begin{matrix}0&&\\&\frac{1}{2}\delta\alpha_3&\\&&0\end{matrix}$	$\begin{matrix}0&&\\&0&\\&&\frac{1}{2}\delta\alpha_3\end{matrix}$			
4	X_4	$\begin{matrix}\frac{1}{2}\delta\alpha_3&&\\&0&\\&&0\end{matrix}$		$\begin{matrix}0&&\\&\frac{1}{2}\delta\alpha_3&\\&&0\end{matrix}$	$-X_4-\frac{1}{2}\delta\alpha_3$		$\begin{matrix}0&&\\&0&\\&&\frac{1}{2}\delta\alpha_3\end{matrix}$		
$\bar{1}$	X_1								
$\bar{2}$	X_2								
$\bar{3}$	X_3		Same as upper right block $\mathbf{v}_0(\bar{i},\bar{j}) = \mathbf{v}_0(i,j)$				Same as upper left block $\mathbf{v}_0(\bar{i},\bar{j}) = \mathbf{v}_0(i,j)$		
$\bar{4}$	X_4								

$$X_1 = \begin{bmatrix} \delta\alpha_1 & \delta\beta_1 & -\delta\beta_1 \\ \delta\beta_1 & \delta\alpha_1 & -\delta\beta_1 \\ -\delta\beta_1 & -\delta\beta_1 & \delta\alpha_1 \end{bmatrix}, \quad X_2 = \begin{bmatrix} \delta\alpha_1 & -\delta\beta_1 & -\delta\beta_1 \\ -\delta\beta_1 & \delta\alpha_1 & \delta\beta_1 \\ -\delta\beta_1 & \delta\beta_1 & \delta\alpha_1 \end{bmatrix}, \quad X_3 = \begin{bmatrix} \delta\alpha_1 & \delta\beta_1 & \delta\beta_1 \\ \delta\beta_1 & \delta\alpha_1 & \delta\beta_1 \\ \delta\beta_1 & \delta\beta_1 & \delta\alpha_1 \end{bmatrix}, \quad X_4 = \begin{bmatrix} \delta\alpha_1 & -\delta\beta_1 & \delta\beta_1 \\ -\delta\beta_1 & \delta\alpha_1 & -\delta\beta_1 \\ \delta\beta_1 & -\delta\beta_1 & \delta\alpha_1 \end{bmatrix},$$

$$X_0 = (m_{Sr} - m_{Ca})\omega^2 - 8\delta\alpha_1$$

TABLE IV. (Unnormalized) mode vectors for an XY_8 complex in the symmetry subspaces given by the decomposition of Eq. (66).

	A_{1g}	E_g		F_{1g}			$F_{2g}(1)$			$F_{2g}(2)$			A_{2u}	E_u		F_{2u}			$F_{1u}(1)$			$F_{1u}(2)$			$F_{1u}(3)$		
0	0	0	0	0	0	0	0	0	0	0	0	0	0	0	0	0	0	0	$4p$	0	0	$-2q$	0	0	0	0	0
	0	0	0	0	0	0	0	0	0	0	0	0	0	0	0	0	0	0	0	$4p$	0	0	$-2q$	0	0	0	0
	0	0	0	0	0	0	0	0	0	0	0	0	0	0	0	0	0	0	0	0	$4p$	0	0	$-2q$	0	0	0
1	-1	-2	0	0	1	1	-1	1	0	-1	0	0	1	2	0	0	1	1	1	0	0	1	0	0	0	-1	1
	-1	1	-1	-1	0	-1	-1	0	1	0	-1	0	1	-1	-1	-1	0	-1	0	1	0	0	1	0	-1	0	1
	1	-1	-1	-1	1	0	0	-1	-1	0	0	-1	-1	1	-1	-1	1	0	0	0	1	0	0	1	1	1	0
2	-1	-2	0	0	1	-1	1	1	0	1	0	0	-1	-2	0	0	-1	1	1	0	0	1	0	0	0	1	1
	1	-1	1	-1	0	-1	-1	0	1	0	1	0	1	-1	-1	1	0	1	0	1	0	0	1	0	1	0	-1
	1	-1	-1	1	1	0	0	-1	1	0	0	1	1	-1	1	-1	-1	0	0	0	1	0	0	1	1	-1	0
3	1	2	0	0	1	-1	1	1	0	-1	0	0	-1	-2	0	0	1	-1	1	0	0	1	0	0	0	-1	-1
	1	-1	1	-1	0	1	1	0	1	0	-1	0	-1	1	1	-1	0	1	0	1	0	0	1	0	-1	0	-1
	1	-1	-1	1	-1	0	0	1	1	0	0	-1	-1	1	-1	1	-1	0	0	0	1	0	0	1	-1	-1	0
4	1	2	0	0	1	1	-1	1	0	1	0	0	1	2	0	0	-1	-1	1	0	0	1	0	0	0	1	-1
	-1	1	-1	-1	0	1	1	0	1	0	1	0	-1	1	1	1	0	-1	0	1	0	0	1	0	1	0	1
	1	-1	-1	-1	-1	0	0	1	-1	0	0	1	1	-1	1	1	1	0	0	0	1	0	0	1	-1	1	0
$\bar{1}$	1	2	0	0	-1	-1	1	-1	0	1	0	0	1	2	0	0	1	1	1	0	0	1	0	0	0	-1	1
	1	-1	1	1	0	1	1	0	-1	0	1	0	1	-1	-1	-1	0	-1	0	1	0	0	1	0	-1	0	1
	-1	1	1	1	-1	0	0	1	1	0	0	1	-1	1	-1	-1	1	0	0	0	1	0	0	1	1	1	0
$\bar{2}$	1	2	0	0	-1	1	-1	-1	0	-1	0	0	-1	-2	0	0	-1	1	1	0	0	1	0	0	0	1	1
	-1	1	-1	1	0	1	1	0	-1	0	-1	0	1	-1	-1	1	0	1	0	1	0	0	1	0	1	0	-1
	-1	1	1	-1	-1	0	0	1	-1	0	0	-1	1	-1	1	-1	-1	0	0	0	1	0	0	1	1	-1	0
$\bar{3}$	-1	-2	0	0	-1	1	-1	-1	0	1	0	0	-1	-2	0	0	1	-1	1	0	0	1	0	0	0	-1	-1
	-1	1	-1	1	0	-1	-1	0	-1	0	1	0	-1	1	1	-1	0	1	0	1	0	0	1	0	-1	0	-1
	-1	1	1	-1	1	0	0	-1	-1	0	0	1	-1	1	-1	1	-1	0	0	0	1	0	0	1	-1	-1	0
$\bar{4}$	-1	-2	0	0	-1	-1	1	-1	0	-1	0	0	1	2	0	0	-1	-1	1	0	0	1	0	0	0	1	-1
	1	-1	1	1	0	-1	-1	0	-1	0	1	0	-1	1	1	1	0	-1	0	1	0	0	1	0	1	0	1
	-1	1	1	1	1	0	0	-1	1	0	0	-1	1	-1	1	1	1	0	0	0	1	0	0	1	-1	1	0

TABLE V. The unperturbed Green's-function matrix $\mathbf{g}^0$ and the defect matrix $\mathbf{v}_0$ in the F_{2g} and F_{1u} symmetry subspaces, as determined from the mode vectors of Table IV.

		F_{2g}		F_{1u}		
		1	2	1	2	3
F_{2g}	1	$B-H+F-U$ $-V-R-Q+2S$	$(V-R-H)\sqrt{2}$			
	2	$(V-R-H)\sqrt{2}$	$B-U-2M-F+2P+Q$			
F_{1u}	1			$8(B+U+2M+F$ $+2P+Q+2p^2A$ $+8pC)/u^2$	$8(B+U+2M+F$ $+2P+Q-A$ $+2C(2p-q))/uv$	$4(H-R-V-4pD)/u$
	2			$8(B+U+2M+F$ $+2P+Q-A+$ $+2(2p-q)C)/uv$	$4(2(B+U+2M+F$ $+2P+Q)+q^2A$ $-8qC)/v^2$	$4(H-R-V+2qD)/v$
	3			$4(H-R-V-4pD)/u$	$4(H-R-V+2qD)/v$	$B+H-F+U+V-R-Q+2S$

		1	2	1	2	3
F_{2g}	1	$-(\delta\alpha_1+\delta\beta_1)$	$\delta\beta_1\sqrt{2}$			
	2	$\delta\beta_1\sqrt{2}$	$-(\delta\alpha_1+\delta\alpha_3)$			
F_{1u}	1			$8(2p^2\delta m\omega^2$ $-\delta\alpha_1(4p-1)^2)/u^2$	$(8/uv)(-\omega^2\delta m$ $+\delta\alpha_1(4p-2q+7))$	$-(4/u)\delta\beta_1(4p-1)$
	2			$(8/uv)(-\omega^2\delta m$ $+\delta\alpha_1(4p-2q+7))$	$(4/v^2)(q^2\omega^2\delta m$ $-2\delta\alpha_1(2q+1)^2)$	$(4/v)\delta\beta_1(1+2q)$
	3			$-(4/u)\delta\beta_1(4p-1)$	$(4/v)\delta\beta_1(1+2q)$	$-(\delta\alpha_1+\delta\beta_1+\delta\alpha_3)$

$p=m_{Ca}/m_F=1/q$, $\delta m=m_{Sr}-m_{Ca}$, $u^2=8(1+2p^2)$, $v^2=4(2+q^2)$

of (67) is just the projection of $\mathbf{v}_0[1+\mathbf{g}^0(\omega+i\epsilon)\mathbf{v}_0]^{-1}$ onto the mode defined by the second set of F_{2g} vectors listed in Table IV. Calculations have been carried out for the first-order PSE that occurs in expression (67) for the Raman intensity, and the results are shown in Fig. 6. These calculations have verified the validity of the conjecture that $\mathbf{g}^0\mathbf{v}_0$ is negligible compared to unity for the Raman mode, and leads to the "virtual-crystal approximation" for the first-order Raman line, as observed (this behavior is related to the real part of the PSE). The linewidth, on the other hand, is related to the imaginary part of the PSE, according to Eq. (67). One of the necessary assumptions that this formalism makes is that the contribution of disordering to the linewidth of mixed crystals is additive with other effects, which are included only phenomenologically by the addition of the term $-i\Gamma_R/2$ which characterizes the pure crystal ($x=0$). The results of the linewidth calculation that were carried out using Eq. (67) and the PSE function of Fig. 6 are shown by the dashed line in Fig. 2- which also contained the experimental data. Note that although the PSE contains considerable structure, the only region where it makes a significant contribution to the Raman intensity is near $\omega_R\sim 326$ cm^{-1}, because of the nearly Lorentzian structure of Eq. (67). In that region, there is a sharp peak in the (imaginary part) of the PSE, and since the prediction of the linewidth is

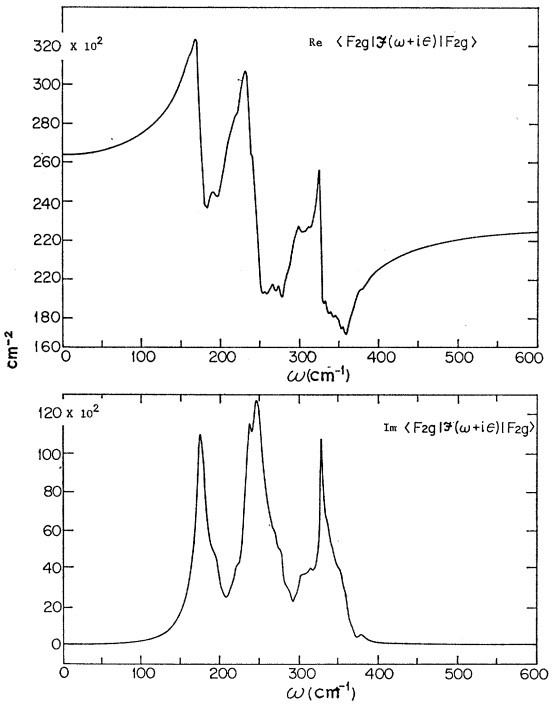

FIG. 6. The ($\mathbf{k}=0$) PSE function that occurs in Eq. (67) for the Raman scattering intensity.

sensitive to the slope of this curve near ω_R, the agreement of the calculation shown in Fig. 2 (by the dashed line) is reasonably good.

B. Infrared Reflectivity

A similar procedure was followed in an attempt to explain the infrared reflectivity data obtained for the $Ca_{1-x}Sr_xF_2$ system by Verleur and Barker.[2] It was assumed that, with the introduction of a Sr^{++} impurity, the first-order electric moment coefficients do not change appreciably from the values $\mathfrak{M}_{\alpha,\mu}{}^0(\kappa)$ that characterize the pure CaF_2 host. That is, we shall again assume that the dominant contribution to the mixed crystal behavior [in this case, the far-infrared dielectric function $\epsilon(\omega)$] comes from the (transverse, TO) $\mathbf{k}\sim 0$ excitations. Then, to lowest order in x for the PSE, the expression (65) for $\epsilon(\omega)$ becomes

$$\epsilon(\omega)/\epsilon_\infty = 1+(\omega_{TO}{}^2-\omega_{LO}{}^2)[\omega^2-\omega_{TO}{}^2+i\Gamma\omega\omega_{TO} +x\langle\sigma_{TO}|\mathbf{M}_0{}^{-1/2}\mathbf{F}^{(1)}(\mathbf{k}=0,\omega+i\epsilon)\mathbf{M}_0{}^{-1/2}|\sigma_{TO}\rangle]^{-1}, \tag{68}$$

where we have, once again, included a phenomenological term $i\Gamma\omega\omega_{TO}$ (conforming to the notation of Verleur and Barker[2]) to account for the damping of the TO frequency of the pure CaF_2 lattice. Thus, we take[2] $\Gamma=0.025$. The value of ϵ_∞ for pure SrF_2 is[70] 2.07, compared to 2.047 for CaF_2, so it is a good approximation to regard ϵ_∞ as a constant in (68). Again, if we appeal to (16) and (41), it is possible to show that, as $\mathbf{k}\to 0$, the PSE in the denominator of Eq. (68) will be the projection of $\mathbf{v}_0[\mathbf{1}+\mathbf{g}^0(\omega+i\epsilon)\mathbf{v}_0]^{-1}$ onto the mode defined by the *second* set of F_{1u} vectors listed in Table IV. (This is a consequence of the convenient choice of $p=m_{Ca}/m_F=1/q$.) The results of the calculation for the PSE that occurs in Eq. (68) are shown in Fig. 7. Equation (68) was used in conjunction with

$$R=\left|\frac{\sqrt{\epsilon(\omega)}-1}{\sqrt{\epsilon(\omega)}+1}\right|^2 \tag{69}$$

to calculate the far-infrared reflectivity spectrum (at normal incidence) for pure CaF_2 and for $Ca_{0.75}Sr_{0.25}F_2$, since these cases can be compared with the experimental observations of Verleur and Barker.[2] The results are displayed in Fig. 8, and although the quantitative agreement is not perfect, there are many qualitative similarities between the theoretical and experimental reflectivities. Note firstly that even for the pure crystal, the present formalism does not describe the reflectivity well (a purely harmonic crystal would have to be 100% reflecting in the reststrahlen region). The inability of a single (damped) mode to adequately describe the pure CaF_2 crystal is an indication of the fact that the crystal may not be well-approximated by a purely harmonic

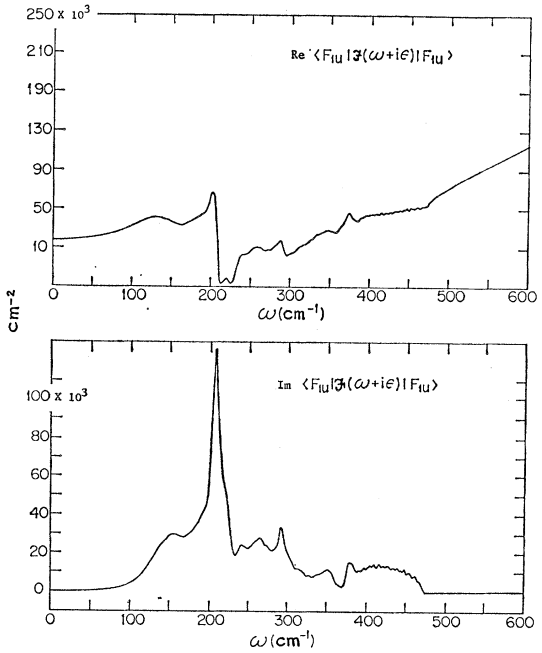

FIG. 7. The ($\mathbf{k}=0$) PSE function that occurs in Eq. (68) for the far-infrared dielectric function $\epsilon(\omega)$.

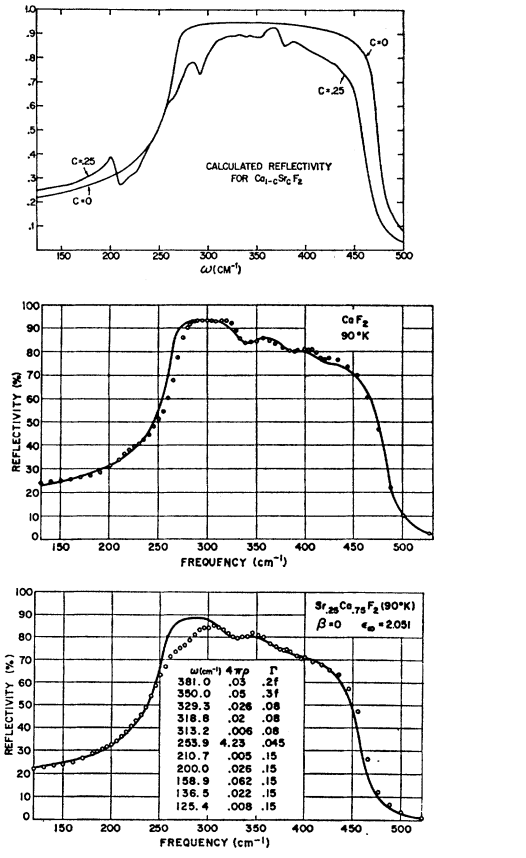

FIG. 8. Theoretical calculations for the reflectivity (top), and experimental results taken from the work of Verleur and Barker, Ref. 2.

solid. The effects of anharmonic processes have been discussed briefly by Bosomworth,[70] who also observes departure from a harmonic lattice in his study of the infrared (IR) absorption in pure CaF_2. In spite of the fact that we do not start with a good theory for the pure crystal, the theoretical curve for the mixed crystal $Ca_{0.75}Sr_{0.25}F_2$ does describe the general decrease of the reflectivity, as compared with the pure crystal, and the rounding off of the edge at 280 cm^{-1}. It also displays a bump near 350 cm^{-1}, as observed. However, there is an anomolous

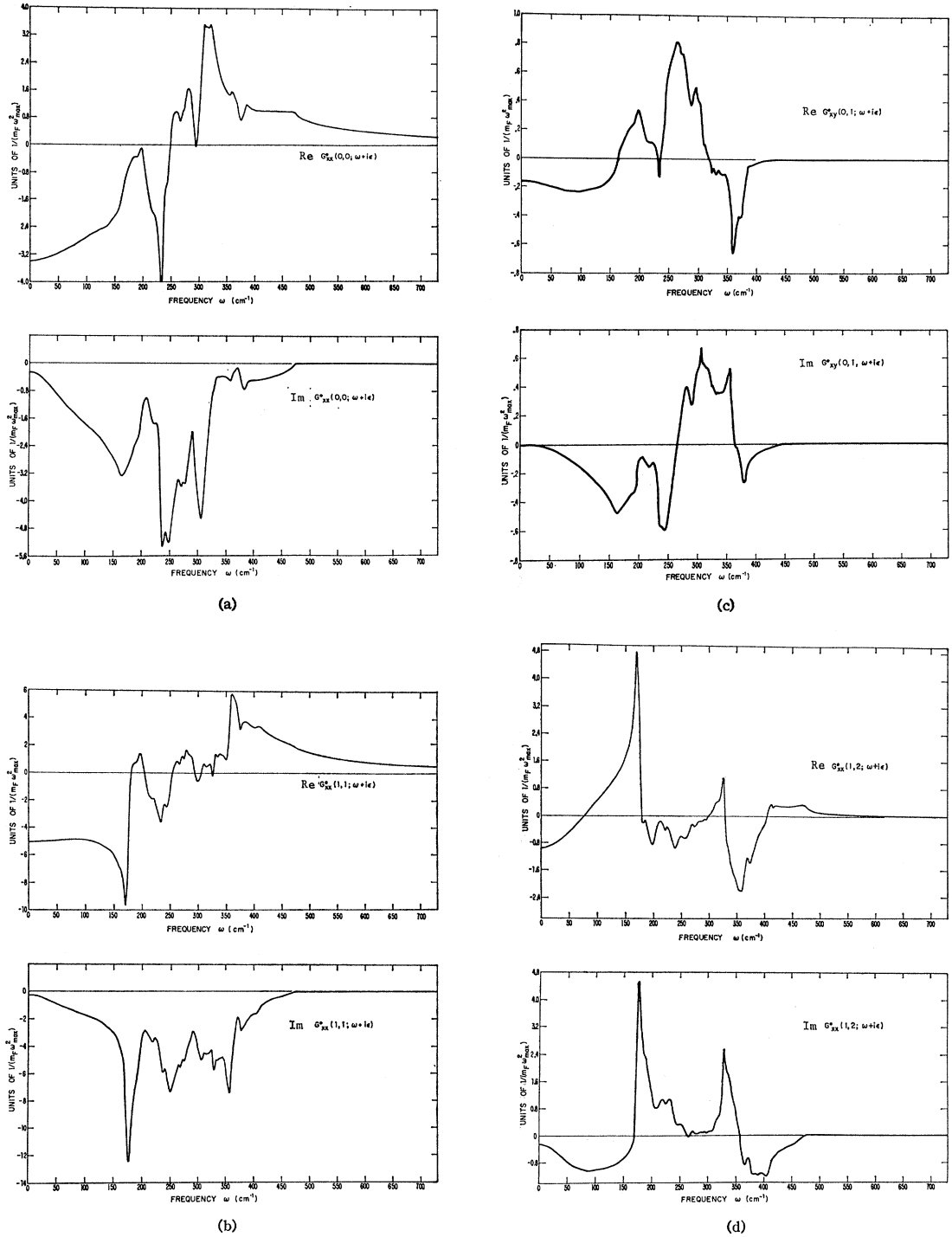

FIG. 9. Real and imaginary parts of the 13 independent Green's functions $g_{\alpha\beta}{}^0$ $(l\kappa, l'\kappa'; \omega+i\epsilon)$ that occur in the XY_8 defect subspace (cf. Fig. 5).

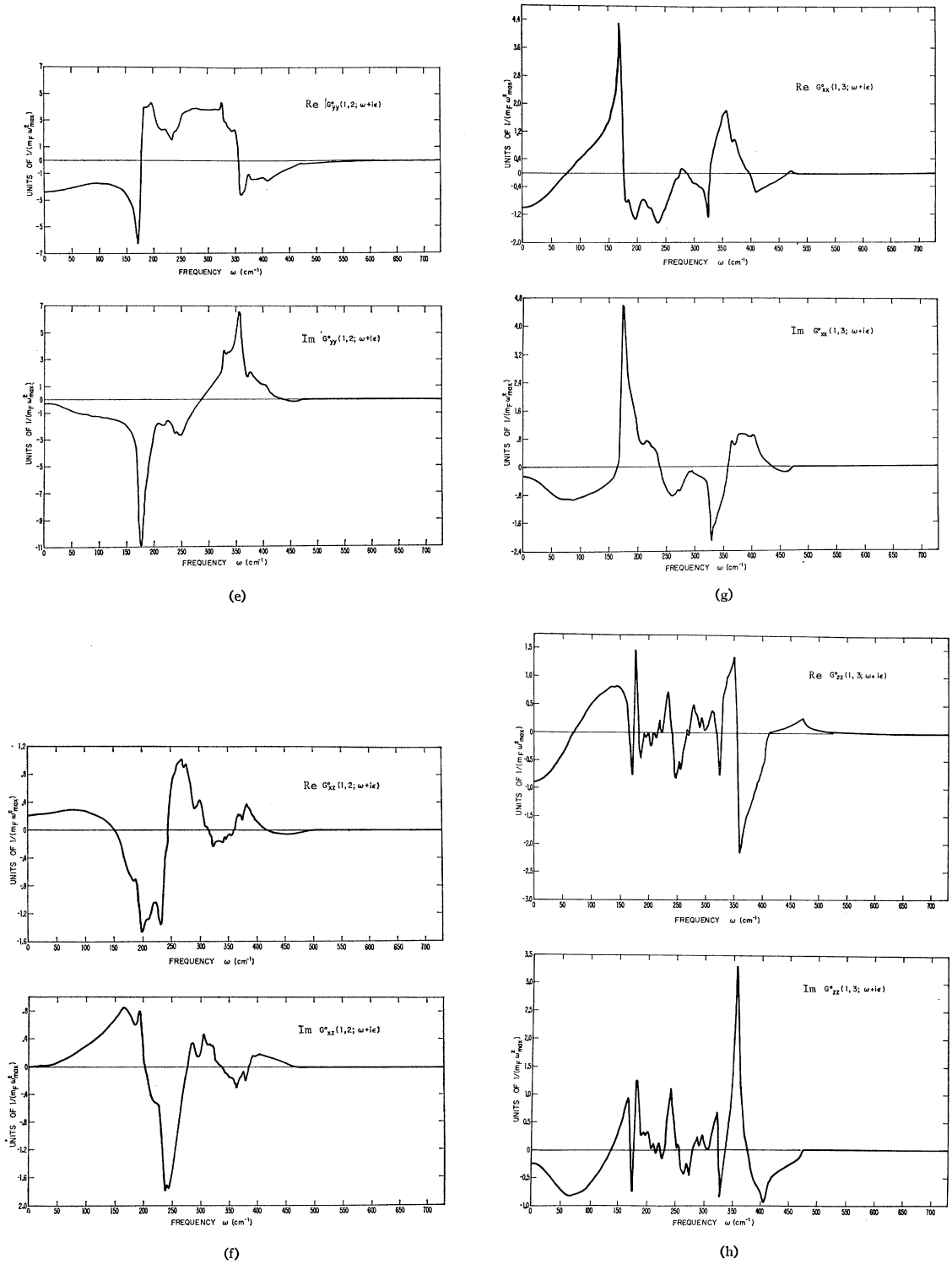

FIG. 9 (*continued*)

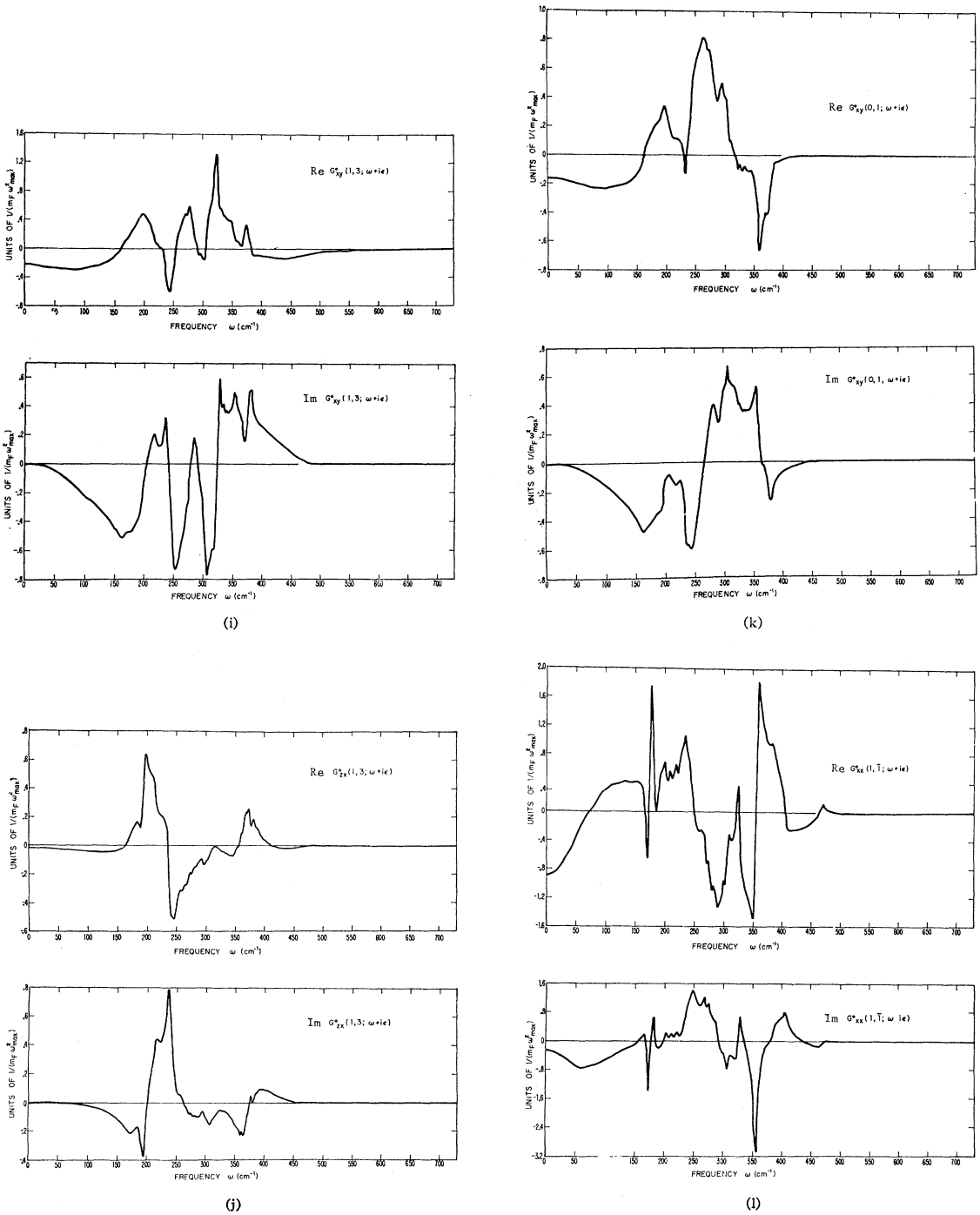

(i) (k)

(j) (l)

FIG. 9 *(continued)*

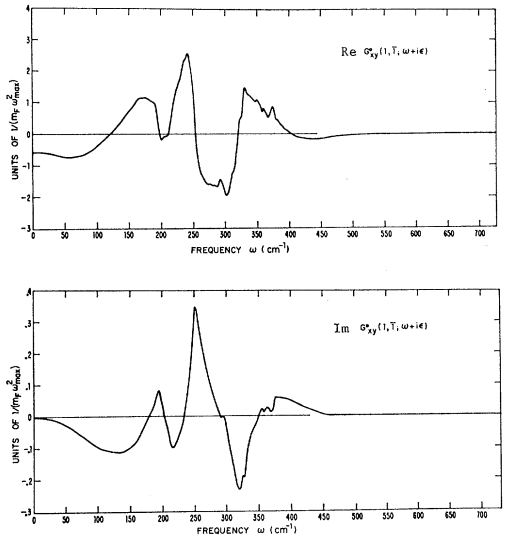

(m)

FIG. 9 (*continued*)

structure at ~ 210 cm^{-1} which corresponds to the sharp peak in the PSE shown in Fig. 7. This coincides with a minimum in the (calculated) density of states for pure CaF_2 (cf. Fig. 4), and is probably an accidental anomayl of the host model. In addition to the fact that anharmonic effects are completely neglected (which is probably the most serious deficiency), it is also possible that the models of the defect or the host are not sufficiently sophisticated. Finally, the assumption that the $\mathfrak{M}^0$ coefficients do not change may be inaccurate, and in that case, there could be a more complicated absorption structure throughout the band.

V. CONCLUSION

In spite of the several quantitative failures of the present calculation, we have demonstrated that, for a reasonably realistic model, the Green's-function formalism does predict the qualitative features that have been observed in the mixed CaF_2-SrF_2 system. Clearly, the present model has not been sufficiently sophisticated to obtain precise quantitative agreement; however, the calculations given here have provided some indication of the difficulties that are involved in describing the phonon optical properties of even reasonably simple disordered systems. It should be clear that significant improvement would be a rather formidable exercise, since realsitic calculations for RS and IR absorption depend upon many different approximations and assumptions.

APPENDIX

The 13 independent Green's functions $g_{\alpha\beta}{}^0(l\kappa, l'\kappa'; \omega+i\epsilon)$ that arise in the XY_8 defect subspace (denoted by $A, B, \ldots, U, V$ in Table II) have been calculated by a histogram technique, using Eqs. (30) and (31). The band of (squared) frequencies was divided into 200 equally spaced intervals, or "bins." It is convenient to calculate the imaginary parts first, using the spectral representation (31), which contains a sum over all $\mathbf{k}$ in the first Brillouin zone (BZ). (The δ functions can be regarded as contributing only to the "bin" in which the frequency $\omega_{\mathbf{k}\sigma}$ lies.) The summation was carried out with a mesh in $\mathbf{k}$ space that included 64 000 points in the first BZ, although exploitation of symmetry made it possible to reduce this sum to 1686 points that lie in the "irreducible" 1/48 zone. After the imaginary parts were calculated as a function of frequency, the real parts were obtained using the Hilbert transform relation (30). FORTRAN IV programs for the IBM 7094 are available[72] for calculation of phonon dispersion curves and Green's functions (based on the rigid-ion model) for the fluorite lattice. For the 1686 point BZ mesh, computation time for the real and imaginary parts of the 13 Green's functions on the IBM 7094 was about 4 h.

[72] W. B. Lacina, thesis, Harvard University, Technical Report, Gordon McKay Laboratory, No. ARPA-36 (unpublished).